

1 **High peatland methane emissions following permafrost thaw: enhanced acetoclastic**
2 **methanogenesis during early successional stages**

3 Liam Heffernan^{1,2*}★, Maria A. Cavaco^{3*}★, Maya P. Bhatia³, Cristian Estop-Aragonés⁴,
4 Klaus-Holger Knorr⁴, David Olefeldt¹

5
6 ¹ Department of Renewable Resources, University of Alberta, Edmonton, AB T6G 2H1,
7 Canada. ² Evolutionary Biology Centre, Department of Ecology and Genetics/Limnology,
8 Uppsala University, Norbyvägen 18D, 752 36, Uppsala, Sweden. ³ Department of Earth and
9 Atmospheric Sciences, University of Alberta, Edmonton, AB T6G 2H1, Canada. ⁴ Institute of
10 Landscape Ecology, Ecohydrology and Biogeochemistry Group, University of Münster,
11 Münster, Germany

12 *Corresponding authors: Liam Heffernan (liam.heffernan@ebc.uu.se) and Maria A. Cavaco
13 (cavaco@ualberta.ca)

14 ★ These authors contributed equally to this work

15
16
17
18
19
20
21
22
23

24 Abstract

25 Permafrost thaw in northern peatlands often leads to increased methane (CH₄) emissions, but
26 ~~gaps remain in our understanding of the~~ underlying controls responsible for increased
27 emissions and the duration for which they persist have yet to be fully elucidated. We assessed
28 how shifting ~~ecological conditions~~ environmental conditions affect microbial communities,
29 and the magnitude and stable isotopic signature ($\delta^{13}\text{C}$) of CH₄ emissions along a thermokarst
30 bog transect in boreal western Canada. Thermokarst bogs develop following permafrost thaw
31 when dry, elevated peat plateaus collapse and become saturated and dominated by *Sphagnum*
32 mosses. We differentiated between a young and a mature thermokarst bog stage (~30 and
33 ~~years~~ ~200 years since thaw, respectively). The young bog located along the thermokarst
34 edge, was wetter, warmer and dominated by hydrophilic vegetation compared to the mature
35 bog. Using high throughput 16S rRNA gene sequencing ~~16S rRNA gene high throughput~~
36 sequencing, we show that microbial communities were distinct near the surface and
37 converged with depth, but lesser differences remained down to the lowest depth (160 cm).
38 Microbial community analysis and $\delta^{13}\text{C}$ data from CH₄ surface emissions and dissolved gas
39 depth profiles show that hydrogenotrophic methanogenesis was the dominant pathway at both
40 sites. However, mean $\delta^{13}\text{C}$ -CH₄ signatures of both dissolved gases profiles and surface CH₄
41 emissions ~~the young bog was~~ found to ~~have be~~ isotopically heavier in the young bog (-
42 63 ‰ and -65 ‰, respectively) compared to the mature bog (-69 ‰ and -75 ‰, respectively)
43 ~~$\delta^{13}\text{C}$ -CH₄ in both dissolved gases profiles and surface CH₄ emissions~~, suggesting that
44 acetoclastic methanogenesis was relatively more enhanced throughout the young bog peat
45 profile. Furthermore, mean young bog CH₄ emissions of 82 mg CH₄ m⁻² day⁻¹, were almost
46 three times greater than the 32 mg CH₄ m⁻² day⁻¹, observed in the mature bog. Our study
47 suggests that interactions between the methanogenic community, and hydrophilic vegetation,
48 warmer temperatures, and saturated surface conditions enhance CH₄ emissions in young

49 ~~thermokarst bog~~ecological conditions and methanogenic communities enhance CH₄
50 emissions in young thermokarst bogs, but that these favorable conditions only persist for the
51 initial decades after permafrost thaw.

52

53 **Keywords**

54 Permafrost, peatland, thermokarst, 16S RNA, isotope, methanogenesis, microbial
55 community, methane emissions

56 **1. Introduction**

57 Methane (CH₄) emissions in northern peatlands are typically thought ~~to be of as being~~
58 driven by environmental and ecological conditions such as temperature, water table position,
59 and vegetation community (Bellisario et al., 1999). However, CH₄ emissions are ultimately
60 the result of microbial activity and understanding the interactions between environmental
61 conditions and microbial processes is key to understanding the impact of disturbances on
62 peatland CH₄ emissions. Increased disturbances such as permafrost thaw are transforming
63 northern latitude peatlands (Helbig, Pappas, & Sonnentag, 2016), through the disruption of
64 the frozen landscape and ~~ecological conditions~~environmental conditions responsible for the
65 regional accumulation of large peatland carbon (C) stores. Rapidly rising northern air
66 temperatures (Mudryk et al., 2018) are predicted to lead to widespread gradual thawing of
67 permafrost (Schaefer et al., 2011) and subsequent thermokarst development in high C density
68 permafrost peatlands (Olefeldt et al., 2016). Thermokarst formation in ice-rich permafrost
69 peatlands is characterized by ground subsidence and surface inundation (Camill, 1999). ~~and~~
70 This exposes previously frozen C to anaerobic microbial decomposition and potential
71 mineralization into greenhouse gases (Schuur et al., 2015). Redox conditions following
72 thermokarst formation are an important control of decomposition, with 3 – 4 times greater C

73 [mineralization occurring as aerobic respiration compared to anaerobic respiration \(Schädel et](#)
74 [al., 2016\)](#). Increased emissions of methane (CH₄) due to thermokarst formation are projected
75 to result in a positive feedback with climate warming (Turetsky et al., 2020). However, the
76 magnitude of peatland CH₄ emissions and the metabolic pathways responsible for these
77 emissions in response to permafrost thaw remain uncertain, as does the period for which
78 these conditions and emissions persist.

79 Methanogenesis, conducted by methanogenic archaea belonging to phylum
80 Euryarchaeota, is one of the most prominent microbial processes contributing to the
81 anaerobic decomposition of organic matter in water-logged permafrost soils (Cai et al., 2016;
82 Knoblauch et al., 2018). Methanogenesis occurs primarily via two pathways: acetoclastic
83 methanogenesis and hydrogenotrophic methanogenesis (Whiticar et al., 1986; Whiticar,
84 1999). Acetoclastic methanogenesis involves the cleavage of acetate into CH₄ and CO₂ and
85 when considering these two species, causes less apparent fractionation than the
86 hydrogenotrophic methanogenesis pathway. This results in acetoclastic methanogenesis
87 yielding comparatively isotopically heavy δ¹³C-CH₄ (δ¹³C = -65 to -50‰). The reduction of
88 CO₂ and H₂ in hydrogenotrophic methanogenesis typically produces CH₄ lighter in ¹³C (δ¹³C
89 = -110 to -60‰) (Hornibrook et al., 1997, 2000). While the two pathways are
90 stoichiometrically equal (Conrad, 1999; Corbett et al., 2013), the activity of acetoclastic and
91 hydrogenotrophic methanogens are governed by different extrinsic controls (Bridgham et al.,
92 2013).

93 [Hydrogenotrophic methanogenesis is thought to be the main pathway of CH₄](#)
94 [formation in northern peatlands \(Hornibrook et al., 1997; Galand et al., 2005\)](#). However, the
95 [acetoclastic pathway can dominate in the upper layers of more minerotrophic, nutrient rich](#)
96 [peatlands \(Popp et al., 1999; Chasar et al., 2000\) where there are sufficient levels of acetate](#)
97 [\(Ye et al., 2012\)](#). ~~Acetoclastic methanogenesis accounts for two-thirds of peatland CH₄~~

98 ~~production in northern peatlands (Conrad, 1999; Kotsyurbenko et al., 2007) and is favoured~~
99 ~~in more minerotrophic, nutrient rich conditions, where there are sufficient levels of acetate~~
100 ~~required to fuel this pathway (Ye et al., 2012).~~ During the initial decades following thaw,
101 surface runoff of nutrients from surrounding intact peat plateaus (Keuper et al., 2012; 2017)
102 and increased connectivity to regional hydrology (Connon et al., 2014), can result in more
103 minerotrophic conditions. ~~These~~ Such shifts in hydrology, temperature, nutrients, redox
104 conditions, and vegetation communities following permafrost thaw have been shown to
105 increase the prevalence of acetoclastic methanogenesis and CH₄ emissions (Hodgkins et al.,
106 2014; McCalley et al., 2014). However, this potential post-thaw enhancement of acetoclastic
107 methanogenesis needs to be considered in context of the existing methanogenic community
108 that developed in the peat profile before thaw. For example, historical ~~ecological~~
109 ~~conditions~~ environmental conditions have been shown to have a legacy effect on the
110 methanogenic community following thaw and can therefore be a key constraint on
111 methanogenic community structure and activity post-thaw (Holm et al., 2020; Lee et al.,
112 2012). Overall, an understanding of the methanogenic community's response following thaw
113 to shifts in both surface conditions and exposure to previously frozen organic matter is key to
114 estimating CH₄ emissions from thermokarst peatlands.

115 Environmental conditions following permafrost thaw in peatlands are characterized
116 by a drastic shift in water table position and increased wetness, increased soil temperatures,
117 and a change in vegetation community associated with increased labile inputs (Beilman,
118 2001; Burd et al., 2020; Camill, 1999). These shifts may provide optimal conditions for CH₄
119 production and emissions, particularly in the initial decades following thaw. Peatland CH₄
120 emissions are constrained by ~~the~~ water table position (Huang et al., 2021; Strack et al., 2004),
121 and surface inundation leads to increased CH₄ emissions (Tuittila et al., 2000). Methane
122 production and emissions are positively influenced by soil temperatures (Hopple et al., 2020;

123 Olefeldt et al., 2017), and peatland CH₄ emissions have been shown to increase when both
124 ~~the~~ water table position and temperatures are high (Grant, 2015). The colonization of
125 vegetation associated with fresh, labile inputs has also been shown to increase both the
126 magnitude and temperature sensitivity of CH₄ emissions in peatlands (Leroy et al., 2017;
127 McNicol et al., ~~2020~~2019). As such, many studies have focussed on the relationship between
128 water table position, soil temperature and vegetation communities in determining CH₄ fluxes
129 following thaw (Johnston et al., 2014; Turetsky et al., 2007; Wickland et al., 2006). However,
130 while these environmental conditions are key drivers of CH₄ emissions, they are unable to
131 fully account for the variability in permafrost peatland CH₄ emissions (Juottonen et al., 2021;
132 Kuhn et al., 2021). Some of this unaccounted variance may be in part explained by microbial
133 activity, as changes in the composition and abundance of methanogenic community members
134 can contribute significantly towards peatland CH₄ emissions (Fritze et al., 2021). Relatively
135 few studies have assessed how shifts in ~~ecological conditions~~environmental conditions and
136 ensuing changes in methanogenic community structure influences CH₄ emissions following
137 thaw (McCalley et al., 2014), an interaction that may be significant both at the local and
138 circumpolar scale.

139 In this study we assess the impact of permafrost thaw on peatland methanogenic
140 community composition and CH₄ emissions along a space-for-time thaw gradient that
141 includes an intact peat plateau and an adjacent thermokarst bog with areas that have thawed
142 ~30 and ~200 years ago (herein referred to as young bog and mature bog, respectively).

143 Thermokarst formation has resulted in distinct environmental conditions at each stage along
144 this thaw gradient. We herein define these distinct environmental conditions as water table
145 position and surface wetness, soil temperatures, and vegetation community. Along this
146 gradient we assessed methanogenic community structure down to 160 cm. We hypothesize
147 that: (1) shifting ~~ecological conditions~~environmental conditions along the permafrost thaw

148 gradient results in a successional microbial community and a restructuring of the
149 methanogenic community, and (2) the warmer conditions [and hydrophilic vegetation](#)
150 [community](#) in the young bog, along with the exposure of previously frozen peat, will result in
151 a greater relative abundance of acetoclastic methanogens throughout the depth profile, and
152 subsequently greater overall CH₄ emissions. In the young bog and mature bog, we measured
153 the concentration and $\delta^{13}\text{C}$ -signature of dissolved CH₄ and CO₂ down to 245 cm, and the
154 rates and $\delta^{13}\text{C}$ -signature of both CH₄ and CO₂ land-atmosphere fluxes. The combined
155 approach of measuring dissolved gas depth profiles and surface emissions, in tandem with
156 assessing the structure of the methanogenic community along a depth profile, allows us to
157 determine how changing ~~ecological conditions~~[environmental conditions](#) following thaw
158 impacts methanogenic pathways and community composition. Utilizing this approach, we
159 can subsequently gain further insight into how long elevated surface CH₄ emissions may
160 persist post-thaw. Furthermore, this approach highlights that while environmental and
161 ~~ecological conditions~~[environmental conditions](#) are important in determining CH₄ emissions,
162 microbial community composition, and changes in the methanogenic community structure
163 are likely to significantly influence CH₄ emissions following thaw.

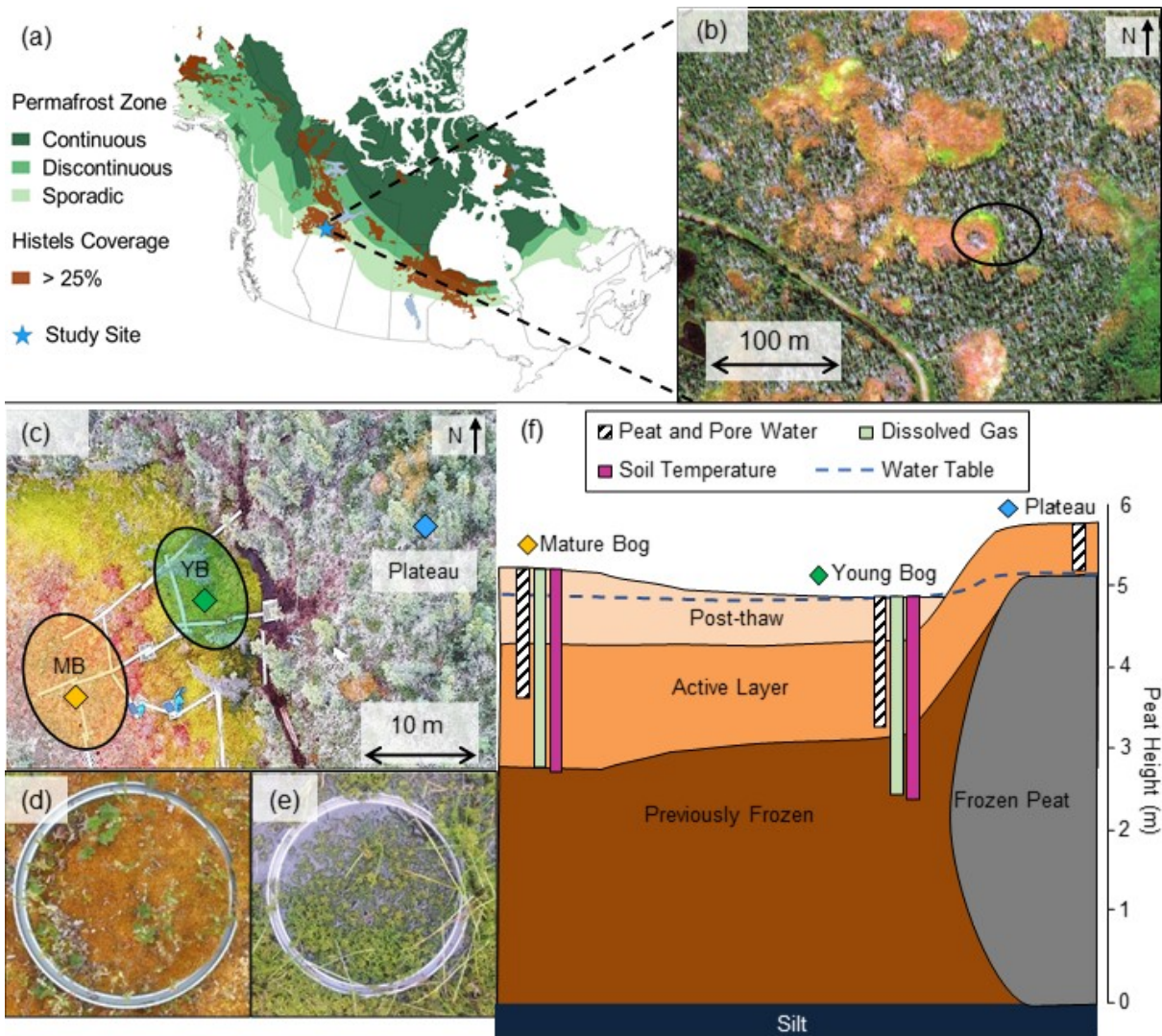
164 **2. Methods**

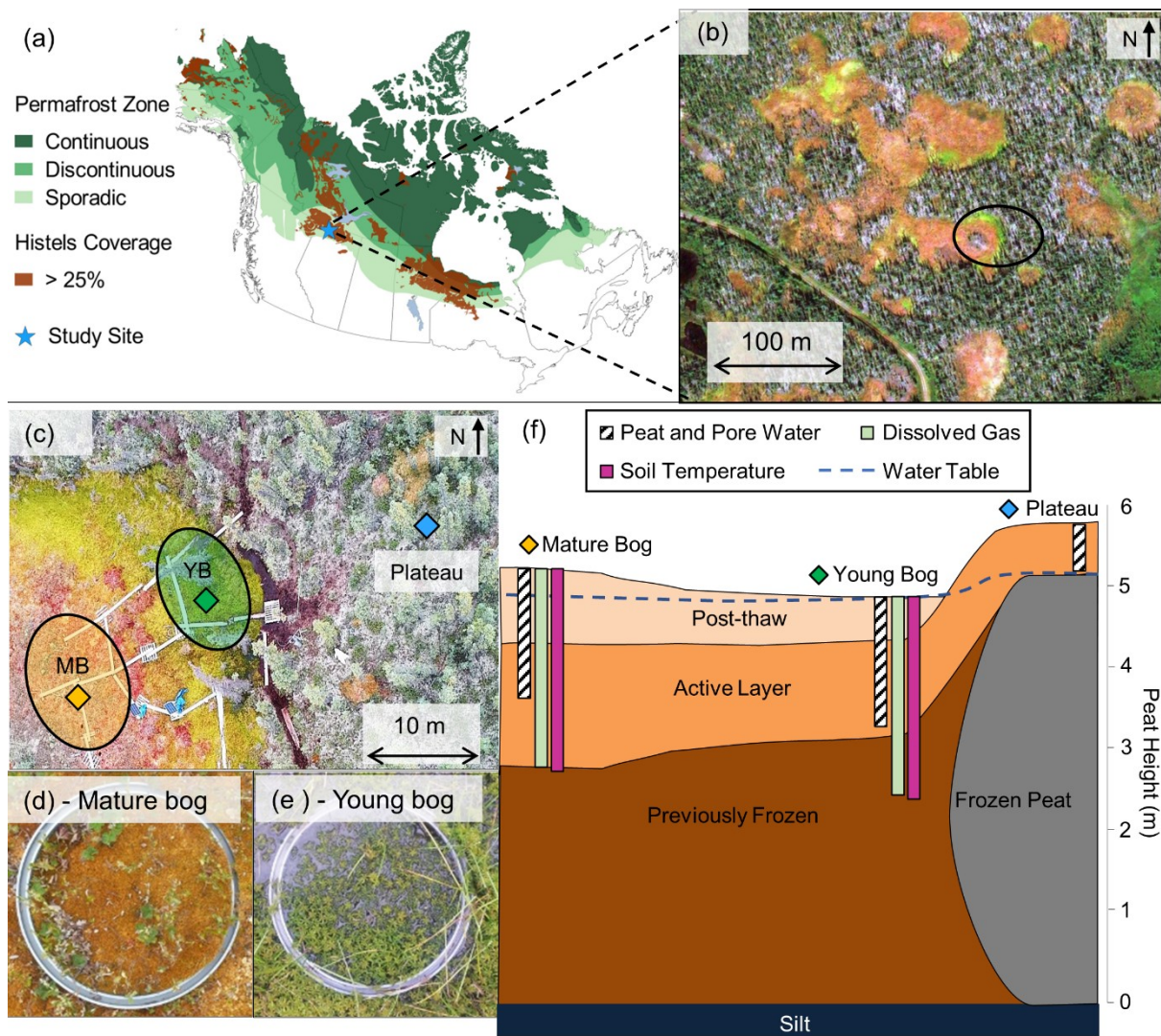
165 *2.1 Study Site and Design*

166 The Lutose peatland study site (59.5°N, 117.2°W; Figure 1) is located on the Interior
167 Plains of western Canada, within the zone of discontinuous permafrost (Brown et al., 1997;
168 Heginbottom et al., 1995). The climate is continental with a monthly average summer high
169 temperature of 16.1 °C (July), winter low of -22.8 °C (January), and annual average air
170 temperature of -1.8 °C (Climate-Data.org, 2019 – data from site located ~50 km south of
171 Lutose). Annual average precipitation is 391 mm, of which three quarters fall as rain between

172 May and September. In the discontinuous permafrost zone of the Interior Plains in boreal
173 western Canada, ~40% of the landscape is covered by permafrost peatlands that have
174 between 2 and 6 m deep peat deposits (Gibson et al., 2018; Vitt et al., 2000). The peatland
175 complexes in this area are a fine-scale mosaic of permafrost peat plateaus, and permafrost-
176 free ponds, fens, and bogs ([Zoltai, 1993](#); [Bauer et al., 2003](#); [Vitt et al., 2000](#); [Pelletier et al.,](#)
177 [2017](#)), and they are similar to those found in the Hudson Bay Lowlands ([Kuhry, 2008](#)) and
178 [Alaska \(Jones et al., 2017\)](#). The Lutose peatland complex is representative of the peatlands
179 found in the discontinuous permafrost zone of the Interior Plains in western Canada ([Zoltai,](#)
180 [1993](#); [Bailman, 2001](#); [Bauer et al., 2003](#); [Vitt et al., 2000](#); [Heffernan et al., 2020](#)). The site has
181 5 – 6 m deep peat and has transitioned through multiple developmental stages since it began
182 accumulating organic matter ~8,800 years ago. It transitioned from a marsh, through a fen
183 and a bog stage prior to permafrost aggradation ~1,800 years ago (Heffernan et al., 2020).

184 [Peatlands in the Interior Plains in western Canada are one of the three largest stores of](#)
185 [organic carbon found in peatlands within the permafrost zone, the other two being the](#)
186 [Hudson Bay Lowlands and the West Siberian Lowlands \(Hugelius et al., 2020; Olefeldt et al.,](#)
187 [2021\)](#). Within the sporadic and discontinuous permafrost zone of our study region >15% of
188 [the total peat plateau area has thawed and formed thermokarst bogs in the last 30 years](#)
189 [\(Baltzer et al., 2014; Gibson et al., 2018\)](#). Projections for this area suggests total permafrost
190 [lost from plateaus by 2050 \(Chasmer and Hopkins, 2017\)](#).





192

193 **Figure 1.** Lutose peatland site location and study design. (a) Site location (Lutose, Alberta,
 194 Canada 59.5°N, 117.2°W) in boreal western Canada. Green shading represents permafrost
 195 zonation (Brown et al., 1997) and brown shading represents areas with >25% permafrost
 196 peatland (histels) extent (Hugelius et al., 2014). (b) Geoeye satellite image of study site
 197 (image from <https://zoom.earth/>), 0.46 m resolution. Circle represents the area where
 198 sampling took place. (c) Aerial image of study transect, locations of peat and dissolved gas
 199 sampling in the plateau (blue diamond), young bog (green diamond), and mature bog (orange
 200 diamond), and area where collars for gas flux measurements were located in the young bog
 201 (YB, green) and mature bog (MB, orange) (Aerial photo credit: Olefeldt, David). (d, e)
 202 Surface vegetation in the mature bog and young bog (f) Soil profile of thaw transect based on
 203 (Heffernan et al., 2020). The transition to Post-thaw peat occurs at 29 cm and 71 cm in the
 204 young bog and mature bog respectively. Peat (core) and pore water (pore water peepers),
 205 including microbial community, sampling depth profile 0 – 160 cm shown as white column
 206 with diagonal black lines. Dissolved gas (diffusive samplers) sampling depth profile 0 – 245
 207 cm shown as light green column. Soil temperature depth profile 0 – 250 cm shown as purple
 208 column. Average water table depth shown as dashed blue line.

209

210 The studied transect represents a space-for-time gradient of permafrost thaw that includes
211 three thaw stages: a permafrost peat plateau, and a young (~30 years since thaw) and mature
212 (~200 years since thaw) part of an adjacent thermokarst bog. The timing of permafrost thaw
213 was previously determined by ¹⁴C dating the shift in macrofossil vegetation indicative of
214 thaw, at 29 cm in the young bog and at 71 cm in the mature bog (Figure 1f) (Heffernan et al.,
215 2020). The peat plateau has an active layer thickness of ~70 cm and its surface is raised 1 – 2
216 m above the adjacent thermokarst bog due to the presence of excess ground ice, resulting in
217 relatively dry surface conditions where the water table generally follows the deepening of the
218 seasonally thawed peat layer (Zoltai, 1972). This thaw stage is characterized by a stunted,
219 open black spruce (*Picea mariana*) canopy and ground cover of lichens (*Cladonia* spp.),
220 *Sphagnum fuscum* hummocks, and low-lying ericaceous shrubs as is characteristic of the peat
221 plateaus in the area (Vitt et al., 1994). The young bog stage is narrow (<5 – 10 m wide) and is
222 located next to the actively thawing area of the peat plateau. The young bog has an average
223 growing season water table position of 1.3 ± 4.9 cm below the peat surface. These inundated
224 conditions result in the dominance of a hydrophilic vegetation community (Figure 1e)
225 consisting of *Sphagnum riparium*, bog-sedge (*Carex limosa*), and rannoch rush (*Scheuchzeria*
226 *palustris*). The mature bog is ~10 – 15 m from the young bog and is relatively drier,
227 compared to the young bog, with an average growing season water table position of $22.9 \pm$
228 9.3 cm below the surface. The dominant vegetation reflects these drier conditions and
229 consists of *Sphagnum fuscum*, *Sphagnum magellanicum*, leather leaf (*Chamaedaphne*
230 *calyculata*), cloudberry (*Rubus chamaemorus*), *Eriophorum vaginatum* tussocks, and some
231 black spruce (*Picea mariana*) regrowth (Figure 1d). The mature bog is located >10 – 20 m
232 from the thawing plateau edge.

233 2.2 Site Preparation and Monitoring of Environmental Conditions

234 The Lutose peatland study site was established in 2015 and a boardwalk was constructed
235 to minimize disturbances along the peat plateau - thermokarst bog transect. Three collars for
236 ~~measurements of surface greenhouse~~ gas fluxes (39 cm diameter) ~~measurements~~ were
237 permanently installed to a depth of 20 cm in both the young and mature ~~thermokarst~~ bog
238 stages. The top of each collar was aligned with the peat surface. PVC wells (2 cm diameter)
239 were installed directly next to each collar and were used to manually monitor the water table
240 position during each gas flux measurement. We monitored soil temperature (°C) at 10, 30, 50,
241 75, 100, 150, 200, and 250 cm every 30 min from May – September 2018 using permanently
242 installed loggers (Hobo 8k Pendant Onset Computer, Bourne, MA, USA) in ~~the young and~~
243 ~~mature bog~~ ~~both thermokarst bog stages~~. Temperature depth profiles were established
244 centrally among collars in each ~~thermokarst~~ bog stage, in areas that had similar vegetation,
245 water table position, and distance from the thawing edge as the collars.

246 Custom made plexiglass pore water suction (Heffernan et al., 2021) and diffusive
247 equilibration gas sampling devices (Knorr et al., 2009) were installed in July 2016 in the
248 young ~~bog~~ and mature bog. These devices were installed in ~~the both young and~~
249 ~~mature thermokarst~~ bog stages, ~1 m from the nearest ~~flux measurement~~ collar. Pore water
250 suction devices were installed to a depth of 160 cm ~~deep~~ and consisted of 15 sampling
251 depths, ~~with each sampling depth~~ connected to the surface via silicone tubing. This allowed
252 for repeated non-destructive pore water sampling. Three diffusive gas sampling devices ~~each~~
253 were installed in ~~the young and mature~~ ~~each thermokarst~~ bog stage, where ~~two two collected~~
254 ~~dissolved soil gas samples collected dissolved soil gas samples~~ from 5 – 95 cm deep and ~~the a~~
255 third from 115 – 245 cm. Each ~~diffusive gas~~ sampler consisted of a PVC pipe with a 10 cm
256 ~~long~~ sampling section centred at each sampling depth. Sampling sections consisted of ~2 m
257 of silicon tubing (3 mm i.d., 5 mm o.d.) wrapped around the PVC pipe and kept in place by
258 PVC-spacers at the top and bottom of each interval. Silicone tubes were sealed at one end

259 whereas the other end was connected to polyurethane tubing (1.8 mm i.d.) that ran back up
260 inside the PVC tube to reach the peat surface where it was sealed with a three-way stopcock.
261 Silicone tubing has been shown to be permeable to gases such as CO₂ and CH₄ within a
262 number of hours, while remaining impermeable to water, making it suitable for sampling of
263 dissolved soil gases (Kammann et al., 2001).

264 *2.3 Pore water chemistry and peat enzyme activity*

265 Pore water dissolved organic matter (DOM) chemistry and peat enzyme activity
266 presented in this study have previously been published (Heffernan et al., 2021), and are
267 briefly described here. Pore water samples for DOM chemistry were taken monthly from
268 May – September 2018 using the previously described pore water suction devices in the
269 young bog and mature bog. Three 60 mL samples were taken from all 15 measurement
270 depths by applying a vacuum at the surface and collecting water with syringes via a three-
271 way stopcock. Each water sample was immediately filtered through 0.7 µm pore size glass
272 fiber filters (GF/F Whatman) into two acid-washed amber glass bottles, with one sample
273 acidified with 0.6 mL 2N HCl to prevent further microbial activity. Pore water samples were
274 transported in a cooled container and stored at 4 °C prior to analysis. Pore water DOM was
275 analyzed for pH, phosphate (PO₄³⁻; µg L⁻¹), dissolved organic carbon (DOC; mg L⁻¹), total
276 dissolved nitrogen (TDN; mg L⁻¹) concentrations, phenolic contents, specific UV absorbance
277 at 254 nm (SUVA, L mg C⁻¹ m⁻¹; Weishaar et al., 2003) and spectral slope between 250 – 465
278 nm (S_{250–465}, nm⁻¹; Helms et al., 2008). SUVA and S_{250–465} values are used to indicate
279 aromaticity, with high SUVA indicating a high aromatic content and lower S_{250–465}
280 indicating low molecular weight and decreasing aromaticity (Hansen et al., 2016).

281 Peat cores extracted to a depth of 160 cm were stored at 4 °C for less than one week in the
282 laboratory before homogenization to determine potential soil enzyme activities. We

283 performed hydrolytic enzyme assays for four enzymes; phosphatase, β -N-glucosaminidase, β -
284 glucosidase, and β -cellobiosidase using fluorogenic 4-methylumbelliferone labelled
285 substrates (Dunn et al., 2014). We assayed oxidative enzyme activity by measuring laccase
286 activity using syringaldazine (Criquet et al., 2000; Jassey et al., 2012). We summarized the
287 activity of all enzymes using a multi-functionality index based on z-scores (Allan et al., 2015;
288 Heffernan et al., 2021).

289 *2.4 Surface Land-Atmosphere Gas Fluxes*

290 We measured surface land-atmosphere greenhouse gas fluxes (CH_4 and carbon dioxide;
291 CO_2) monthly from May – September 2018 at the 3 collars in each peatland stage using the
292 static chamber method (Carroll & Crill, 1997). The chamber used to capture land-atmosphere
293 fluxes was a transparent cylindrical Plexiglass chamber with a basal area of 0.12 m^2 , height
294 of 0.40 m, and volume of 47.8 L. The chamber was equipped with three fans (Micronel
295 Ventilator D341T012GK-2, BEDEK GmbH, Dinkelsbühl, Germany) to mix air during
296 measurements and a temperature sensor (Hobo RH Smart Sensor, S-THB-M002, Onset
297 computers, Bourne, USA) that was shaded from direct sunlight (Burger et al., 2016). An
298 airtight seal was formed between the chamber and collar by pouring water in a $\sim 1.5 \text{ cm}$ deep
299 well around the upper circumference of each collar. Land-atmosphere fluxes of CO_2
300 (ecosystem respiration) and CH_4 were captured simultaneously in darkened conditions by
301 covering the chamber with a reflective shroud. Gas concentrations were determined at a
302 temporal resolution of 1 s using an Ultraportable Greenhouse Gas Analyser (Los Gatos
303 Research, CA, USA) and real-time fluxes were monitored using the VNV® Viewer
304 (RealVNC® Limited, UK) application with an iPad mini 2 (Apple Inc.).

305 The rates of CH_4 and CO_2 land-atmosphere fluxes (*Flux*) were calculated using ~~the~~
306 ~~change in gas concentration over time inside the chamber (linear regression)~~; the ideal gas

307 law following, average air temperature inside the chamber during the measurement, and a
 308 constant atmospheric pressure value of 0.96 atm in Eq. (1):

$$309 \quad Flux = slope \frac{P.V}{R.T.A} \quad (1)$$

310 where slope is the linear rate of change of gas concentration ($\mu\text{mol mol}^{-1} \text{second}^{-1}$) over the
 311 measurement period inside the chamber; P is an atmospheric pressure (atm) constant of 0.96
 312 atm; V is chamber volume (L); R is the universal gas constant ($\text{L atm K}^{-1} \text{mol}^{-1}$); T is the
 313 average temperature (K) inside the chamber during the measurement; and A is the chamber
 314 basal area (m^2). Chamber closure for each flux measurement was 5 minutes with the first 2
 315 minutes discarded to ensure fluxes (i.e., change in concentration over time) with $R^2 > 0.75$.
 316 We report CO_2 fluxes in $\text{g CO}_2 \text{m}^{-2} \text{day}^{-1}$ and CH_4 fluxes in $\text{mg CH}_4 \text{m}^{-2} \text{day}^{-1}$, with positive
 317 values indicating fluxes to the atmosphere. To quantify the proportion of C being emitted as
 318 CH_4 , we standardized our CO_2 and CH_4 fluxes per g C emitted. The proportion of C emitted
 319 as CH_4 ($\text{CH}_4:\text{C}$ emissions) was calculated as

320 Slope is the linear rate of change of gas concentration ($\mu\text{mol mol}^{-1} \text{second}^{-1}$) over the
 321 measurement period inside the chamber; P is atmospheric pressure (atm); V is chamber
 322 volume (L); R is the universal gas constant ($\text{L atm K}^{-1} \text{mol}^{-1}$); T is the temperature (K); and A
 323 is the chamber basal area (m^2). Chamber closure for each flux measurement was 5 minutes
 324 with the first 2 minutes discarded to ensure fluxes (i.e., change in concentration over time)
 325 with $R^2 > 0.75$. We report CO_2 fluxes in $\text{g CO}_2 \text{m}^{-2} \text{day}^{-1}$ and CH_4 fluxes in $\text{mg CH}_4 \text{m}^{-2} \text{day}^{-1}$;
 326 with positive values indicating fluxes to the atmosphere. To quantify the proportion of C
 327 being emitted as CH_4 we standardized our CO_2 and CH_4 fluxes per g C emitted. The
 328 proportion of C emitted as CH_4 was calculated as

$$329 \quad \text{CH}_4:\text{C emissions} = \frac{\text{g C CH}_4 \text{m}^{-2} \text{day}^{-1}}{\text{g C CO}_2 \text{m}^{-2} \text{day}^{-1} + \text{g C CH}_4 \text{m}^{-2} \text{day}^{-1}}$$

330 $\delta^{13}\text{C-CH}_4: C \text{ emissions} = \frac{\text{CH}_4 \text{ m}^{-2} \text{ day}^{-1}}{\text{CH}_4 \text{ m}^{-2} \text{ day}^{-1} + \text{CO}_2 \text{ m}^{-2} \text{ day}^{-1}}$
 331 (2)

332 2.5 $\delta^{13}\text{C}$ -signature of CH_4 emissions

333 We assessed the $\delta^{13}\text{C}$ - CO_2 and $\delta^{13}\text{C}$ - CH_4 signatures of ecosystem respiration (CO_2) and
 334 CH_4 emissions. This was done similarly to regular measurements of CO_2 and CH_4 fluxes, but
 335 using a smaller, opaque chamber of 31.1 L and discrete syringe-samples for $\delta^{13}\text{C}$ analysis in
 336 combination with the continuous monitoring of gas concentrations described above. Gas
 337 syringe samples were taken using a 20 mL syringe via a three-way stopcock placed between
 338 the sealed chamber and gas inlet port on the Ultraportable Greenhouse Gas Analyser. Gas
 339 samples were then injected into a 37.5 mL sealed glass-vial that had been flushed with
 340 nitrogen gas prior to sealing. Chamber enclosure time ranged from 30 – 50 minutes with 4 – 5
 341 samples being taken during this time. Samples were taken either every 10-minutes or once a
 342 minimum change in CO_2 ($30 \mu\text{mol mol}^{-1}$) and CH_4 ($1 \mu\text{mol mol}^{-1}$) concentrations was
 343 observed. An atmospheric gas sample was used as a time-zero measurement when assessing
 344 the change in concentration over time. Glass-vials containing samples were stored at 4°C
 345 until analysis. These measurements were taken in September and October 2016 from 1 collar
 346 in both the young and mature bog, with each collar measured twice.

347 We measured the $\delta^{13}\text{C}$ values of gas samples from both the chamber fluxes and
 348 atmospheric background. Gas vials containing both the chamber and atmospheric gas samples
 349 were analysed in the laboratory for ^{13}C isotopic signatures. To assess whether the gas
 350 concentration of each sample fit within the measurement range required for $\delta^{13}\text{C}$ analysis we
 351 measured CO_2 and CH_4 concentrations using 1 – 3 mL from each vial. Concentrations of CO_2
 352 and CH_4 , using between 1 – 3 mL from each vial, were checked in order to validate the
 353 tightness of the containers and to ensure that concentrations fit within the measurement

354 range required for ^{13}C analysis. Subsequently, after measurement of the concentration of CO_2
355 and CH_4 in each sample. Following these concentration measurements, the ^{13}C - CO_2 and ^{13}C -
356 CH_4 signature was quantified in-line with a cavity ring-down spectrometer (G2201-L,
357 Picarro, California, USA) that had been calibrated using certified standards. To this end, the
358 remaining sample (17 – 19 ml) was diluted with nitrogen gas to a final volume of 20 mL and
359 injected for analysis into a Small Sample Introduction Module (SSIM, Picarro, California,
360 USA) system to measure $\delta^{13}\text{C}$ signatures. The $\delta^{13}\text{C}$ - CO_2 and $\delta^{13}\text{C}$ - CH_4 signature was
361 measured in-line with a cavity ring-down spectrometer (G2201-L, Picarro, California, USA)
362 that had been calibrated using certified standards.

363 We then used the time-series of $\delta^{13}\text{C}$ - CH_4 and CH_4 concentrations to estimate the $\delta^{13}\text{C}$ -
364 CH_4 signature of the CH_4 released to the atmosphere using Keeling plots (Keeling, 1958).
365 Using this approach, the $\delta^{13}\text{C}$ - CH_4 signature of gas in each sample is plotted on the y-axis
366 against the inverse of CH_4 gas concentrations ($1/[\text{CH}_4]$). The y-axis intercept of the linear
367 regression represents the mean isotopic signature of the CH_4 source (Fisher et al., 2017).
368 While fractionation during diffusive transport may influence these estimates, it has been
369 shown in similar systems to be of minor importance compared to other contributing processes
370 (Preuss et al., 2013; Nielsen et al., 2019).

371 2.6 Dissolved gas depth profiles

372 Dissolved gas samples were ~~taken~~ collected using the diffusive equilibration gas
373 sampling devices. Samples were taken from ~~the following~~ 15 depths: ~~that include 5 –~~
374 ~~15 cm and then~~ every 10 cm down to 95 cm starting at 5 – 15 cm down to 95 cm, and then at
375 115 cm, 140 cm, 165 cm, 195 cm, and 245 cm. Once a month from May – September 2018 a
376 Samples of ~7 mL gas sample were was drawn from each depth ~~monthly from May –~~
377 ~~September in 2018~~ using a 10 mL plastic syringes. These gas Samples samples were
378 immediately injected into a 10 mL sealed glass-vial that had been flushed with nitrogen gas

379 prior to sealing, and then were ~~Glass vials containing~~ These gas samples were stored at 4 °C
380 until analysis. ~~A total of Concentrations of 214 dissolved~~ CO₂ and ~~211 CH₄ dissolved for~~
381 ~~each gas concentration measurements were made s~~ were analysed ~~measured by injecting 1 – 3~~
382 ~~mL of gas into using~~ a gas chromatograph with an FID and CO₂ methanizer (8610C Gas
383 Chromatograph, SRI Instruments, California, USA). ~~for a total of 214 and 211 concentrations~~
384 ~~of CO₂ and CH₄, respectively. Between 1 – 3 mL of gas was injected into the analyser. We~~
385 ~~measured Signatures of $\delta^{13}\text{C}$ -CO₂ and $\delta^{13}\text{C}$ -CH₄ signatures using~~ were measured with the
386 previously mentioned ~~method using the~~ cavity ringdown spectrometer and SSIM system. As
387 with surface ~~chamber~~ gas samples, dissolved gas samples were diluted with N₂ to 20 ml.
388 However, dissolved gas concentrations were considerably higher than gas concentrations
389 found in the surface chambers, and some were well above the ~~optimal range~~ concentration
390 ~~range~~ required for accurate $\delta^{13}\text{C}$ analysis for the SSIM system even after dilution. ~~Due To fit~~
391 ~~withinto the optimal operational CH₄ concentration range of the SSIM measurement range of~~
392 ~~the system, m used,~~ further dilution ~~of samples to CH₄ concentrations within the systems~~
393 ~~measurable range~~ resulted in CO₂ concentrations below detectable limits. As such, we were
394 able to obtain 90 and 75 measurements of $\delta^{13}\text{C}$ -CH₄ in the young and mature bog,
395 respectively, and 93 measurements of $\delta^{13}\text{C}$ -CO₂ in both.

396 We used the $\delta^{13}\text{C}$ -CO₂ and $\delta^{13}\text{C}$ -CH₄ signature of each gas sample to calculate the
397 apparent fraction factor α_c , where $\alpha_c = [^{13}\text{C}\text{-CO}_2 + 1000]/[^{13}\text{C}\text{-CH}_4 + 1000]$. The α_c can serve
398 as an isotopic indicator of the pathway of methanogenesis, with typical values of 1.060 –
399 1.090 observed for hydrogenotrophic methanogenesis and 1.040 – 1.060 for acetoclastic
400 methanogenesis (Chanton et al., 2005).

401 *2.7 Peat and pore water sample collection for microbial community composition*
402 *analyses*

403 Microbial community composition was characterized in both peat and peat pore water
404 samples from depths between 0 – 160 cm in the young bog and mature bog. Focussing on
405 peat samples, microbial community composition in the active layer of the peat plateau was
406 assessed from depths between 0 – 30 cm. Peat cores were extracted in June and September
407 2018. Near-surface cores were extracted using a cutting tool to 30 cm deep in the peat plateau
408 and young bog, and 50 cm deep in the mature bog. Surface cores were limited to 30 cm in the
409 plateau due to the presence of ground ice during sampling in June. Surface core depths
410 differed between the young bog and mature bog due to differences in the water table position.
411 Deeper core sections (down to 160 cm) in the young bog and mature bog were extracted
412 using a Russian peat corer (4.5 cm inner-diameter, Eijkelkamp, Giesbeek, The Netherlands).
413 Cores were extracted from two boreholes located ~20 cm apart, alternating between
414 boreholes to avoid disturbance contamination from the 10 cm corer tip during the coring
415 process. To do so, 50 cm long core sections were taken alternatively from each borehole, with
416 each core having a 10 cm overlap with the previous core taken from the adjacent borehole. In
417 the field, immediately after the entire core was extracted, cores were divided into 15
418 subsections. The first two subsections contained peat from 0 – 5 cm and 5 – 10 cm, followed
419 by 10 cm increments down to 120 cm, and two further subsections from 130 – 140 cm and
420 150 – 160 cm. Peat from each interval was sub-sampled using sterilized forceps and placed
421 directly into Whirl-Pak® bags, and frozen within 3 hours of sampling for transportation back
422 to the laboratory. Once samples reached the laboratory, they were frozen at -80 °C until
423 analysis.

424 We also sampled peat pore water at all 15 peat sampling depths in September 2018 from
425 the pre-installed pore water suction sampling devices mentioned above. We extracted 60 mL
426 pore water samples by applying a vacuum at the surface and collecting water with new plastic
427 60 mL syringes. Pore water was immediately filtered through sterile 0.2 µM pore size

428 [Polyvinylidene difluoride \(PVDF\)](#) ~~PVDF~~ membrane sterivex filters (MilliporeSigma).
429 Microbial cells were retained on the filter, and remaining porewater in the sterivex was
430 removed via extrusion using a 60 mL sterile syringe. Sterivex filters were then immediately
431 flash-frozen at -80 °C in a liquid nitrogen dry-shipper to preserve microbial community
432 members until analysis could take place.

433 *2.8 DNA extraction*

434 [Microbial Genomic](#) DNA was extracted from all peat and pore water samples using the
435 DNeasy PowerSoil kit (Qiagen) and the PowerWater DNeasy kit (Qiagen), respectively, to
436 assess the differences in microbial community structure. Extraction of DNA from both
437 sample types was followed as described by the manufacturer (Qiagen), with two
438 modifications: (i) for peat samples, prior to mechanical lysis using bead beating, the prepared
439 samples were chemically lysed by incubation at 70 °C for 10 minutes in the provided lysis
440 solution, and (ii) sterivex (pore water) samples were incubated with rotation at 37 °C
441 following addition of lysis buffer. These modifications were made to increase total DNA
442 yield. The amount of isolated DNA from each sample was then determined using a Qubit
443 fluorometer (model 2.0, using the 1×HS dsDNA kit), with concentrations ranging between
444 ~0.1 and 22.4 ng μL^{-1} . This extracted DNA served as the template for polymerase chain
445 reaction (PCR) analyses described below.

446 *2.9 Sequencing and computational analyses*

447 We amplified 16S rRNA genes using universal prokaryotic primers 515F (Parada, Needham
448 & Fuhrman, 2016) and 926R (Quince et al., 2011). Each primer also contained a six-base
449 index sequence for sample multiplexing (Bartram et al., 2011). The PCR mix (25 μL total
450 volume) contained 1 \times Q5 reaction buffer, 0.5 μM forward primer, 0.5 μM reverse primer,
451 200 μM dNTPs, 0.500 U Q5 polymerase (New England Biolabs, Ipswich, M.A, U.S.A) and
452 2.5 μL of genomic template. Genomic extracts with DNA concentrations of greater than 2 ng

453 μL^{-1} were diluted 1:100 in nuclease-free water. The PCR was performed as follows: 95 °C for
454 3 minutes, 35 cycles of 95 °C for 30 seconds, 60 °C for 30 seconds, 70 °C for 1 minute and a
455 final extension of 70 °C for 10 minutes. Pooled 16S rRNA gene amplicons were purified
456 using Nucleomag beads and a 4.5 pM library containing 50% PhiX Control v3 (Illumina,
457 Canada Inc., NB, Canada) was sequenced on a MiSeq instrument (Illumina Inc., CA, USA)
458 using a 2 × 250 cycle MiSeq Reagent Kit v3 (Illumina Canada Inc) at the Molecular Biology
459 Service Unit (MBSU, University of Alberta). The MiSeq reads were demultiplexed using
460 MiSeq Reporter software version 2.5.0.5. Each read pair was assembled using the paired-end
461 assembler for Illumina sequences (PANDAseq; Masella, Bartram & Truszkowski, 2012) with
462 a quality threshold of 0.9, dictating that 90% of overlapping reverse and forward reads must
463 match in order to assemble reads into read pairs. Assembled reads were analyzed using the
464 Quantitative Insights Into Microbial Ecology II pipeline (QIIME2; Boylen et al., 2020).
465 Sequences were clustered into amplicon sequence variants (ASVs) with chimeric sequences,
466 singletons and low abundance ASVs removed using DADA2 (Callahan et al., 2019). All
467 representative sequences were classified with the Greengenes reference database, using the
468 most recent release (version 13.8; McDonald et al., 2012). [Although Greengenes is not](#)
469 [updated as frequently as the SILVA database, we chose to use it to classify our ASVs as a](#)
470 [comparison of both databases revealed that they captured a similar number of archaea \(total](#)
471 [of 51187 methanogenic read counts attributed to SILVA versus 51141 methanogenic read](#)
472 [counts attributed to Greengenes\). The taxonomic resolution between both databases was also](#)
473 [similar, identifying the same kinds of phyla, families and genus, and methanogens \(e.g.,](#)
474 [methanoregula, methanosarcinales, etc. . . .\), etc. . . .\) Given these similarities, and the fact that](#)
475 [methanogen nomenclature has not changed significantly over time, we ultimately chose to](#)
476 [use Greengenes because it was able to resolve more methanogenic families belonging to](#)
477 [Methanocellales and Methanomassiliicoccaceae particularly, compared to SILVA. The](#)

478 [Greengenes database](#) is also [still commonly used to explore methanogenic archaeal](#)
479 [communities](#) in current literature ([Vanwonderghem et al., 2016](#), [Lin et al., 2017](#), [Carson et al.,](#)
480 [2019](#)). Furthermore, ~~Because~~ since [1021 methanogenic reads were captured per sample](#), on
481 average, [using Greengenes and are comparable to other studies](#) ([Vishnivetskaya et al., 2018](#);
482 [Holm, et al., 2020](#)) ~~we believe that our approach is sufficient for covering methanogen~~
483 [diversity](#).

484 485 2.10 *Statistical analyses*

486 All statistical analyses were carried out in R (Version 3.4.4, R Core Team, 2015) using
487 the *nlme*, *vegan*, *factoextra*, *ggplot2*, *VariancePartition* and *ggpubr* packages (Pinheiro et al.,
488 2017; Oksanen et al., 2013; Kassambara & Mundt, 2017; Wickham, 2016; Hoffman &
489 Schadt, 2016; Kassambara, 2018). For Analysis of Variance (ANOVAs), distribution of the
490 data was inspected visually for normality along with the Shapiro-Wilk test. We tested
491 homogeneity of variances using the *car* package and Levene's test (Fox and Weisberg, 2011).
492 We report uncertainty as ± 1 standard deviation, except for land-atmosphere greenhouse gas
493 fluxes which we report as $\pm 95\%$ confidence intervals. We here define the statistical
494 significance level at 5%.

495 We used ANOVAs and Bonferroni post-hoc tests on linear mixed effects models to
496 [address our second hypothesis and to](#) evaluate significant differences and seasonal trends in
497 greenhouse gas fluxes and dissolved gas depth profiles. ~~These were~~ We performed ~~with a~~
498 [focus on assessing these tests to assess](#) whether thaw stage (young bog or mature bog)
499 influenced greenhouse gas fluxes and dissolved gas depth profiles. This approach was used to
500 test for significant differences in CH₄ fluxes, ratio of CH₄:C emissions, and source ¹³C-CH₄
501 signature intercepts of Keeling plots between young bog and mature bog stages. In each
502 linear mixed effect model, sampling month and peatland stage were defined as fixed effects
503 whereas sampling collar was defined as a random effect. Similarly, we ~~assessed~~ [tested](#) for

504 significant differences [between the in-depth profiles young and mature bog depth profiles with](#)
505 [respect to ~~of~~ dissolved CH₄ and CO₂ concentrations, δ¹³C-CH₄ and δ¹³C-CO₂](#)
506 [signatures values, and ~~α_c values, and pore water chemistry.~~ between the young bog and mature](#)
507 [bog.](#) In these models, sampling month and peatland stage were defined as fixed effects while
508 sample depth was defined as a random effect.

509 Following microbial 16S rRNA gene sequencing ~~on an Illumina Miseq~~, sample reads
510 were rarefied to the lowest read count of 28,129 for all subsequent analyses. These sequences
511 represent whole microbial community data that was used to determine whether there was
512 evidence of changes in microbial community structure representing the successional peatland
513 stages following permafrost thaw throughout the 160 cm depth peat profile. In addition, [to](#)
514 [address our first hypothesis,](#) ~~s~~ we assessed differences in community composition across both
515 peat and pore water and to determine whether seasonality impacted microbial community
516 structure in both sample matrices. Here, Bray Curtis dissimilarity matrices for overall
517 microbial community data were used, at 999 permutations, to identify distinct groupings
518 assessed at the 95% confidence interval in NMDS ordinations. These distinct groupings were
519 further evaluated for significance using the non-parametric [Analysis of](#)
520 [Similarities](#) ~~permutational analysis of variance (PERMANOVA) (ANOSIM)~~ test.

521 [To further test our first hypothesis,](#) ~~Methanogens-methanogens~~ were selected at the
522 order level from our whole community data using Greengenes-assigned taxonomy. Utilizing
523 their assigned taxonomy, the pathways through which identified methanogens conduct
524 methanogenesis was determined by comparing our findings with the literature (Berghuis et
525 al., 2019; Stams et al, 2019; [Kendall & Boone, 2006; Zhang et al., 2020](#)). Focusing on the
526 methanogenic community allowed us to specifically assess how permafrost thaw affects the
527 microbial community responsible for CH₄ production and net CH₄ emissions following thaw.
528 We utilized our methanogenic community data to construct redundancy analyses (RDA) and

529 relative abundance bar plots. RDAs were conducted using a Hellinger-transformed
530 methanogenic community. Explanatory variables (i.e., dissolved concentrations of CO₂, CH₄,
531 DOC, temperature, enzymatic activity estimate, thaw stage, depth, and distance to water
532 table) were scaled about the mean. These explanatory variables had variance standardized,
533 were checked for collinearity (parameters with variance inflation value > 10 were removed)
534 and selected for significance using backward selection, set at 1,000 permutations. The
535 significance of the RDA model, and of each axis was tested using ANOVAs, set at 999
536 permutations. Variance partitioning analyses were conducted to assess the contribution of
537 significant environmental parameters (i.e., thaw stage and distance to water table) on the
538 structuring of the Hellinger-transformed methanogenic community. Distance from water table
539 reflects the distance (in cm) a certain sample is from the water table in different stages of
540 thaw (young bog and mature bog). Due to the smaller size of our methanogenic community
541 relative to the total community, and the lack of some data at certain depths, we combined
542 pore water and peat samples together for these analyses. Relative abundance, which measures
543 how common or rare a particular microorganism is relative to ~~others in~~ the entire microbial
544 community, of methanogenic orders related to acetoclastic or hydrogenotrophic
545 methanogenesis processes were plotted according to depth. Significant differences in
546 methanogenic community composition between depths were assessed using the non-
547 parametric Kruskal-Wallis test with a Benjamini-Hochberg correction for multiple
548 comparisons, after running a Wilcoxon rank sum test.

549 **3. Results**

550 *3.1 Site environmental conditions*

551 The young bog was wetter and warmer than the mature bog throughout the May –
552 September 2018 study period. In June, following snowmelt, the water table was at its highest

553 at 2.2 ± 0.6 cm above the surface in the young bog. The highest water table position in the
554 mature bog was 17.5 ± 1.9 cm below the peat surface and observed in July. The water table
555 dropped during the season and in September was 5.7 ± 2.2 cm and 27.3 ± 1.2 cm below the
556 peat surface, in the young bog and mature bog respectively. In the plateau, the seasonally
557 thawed layer gradually deepened during the growing season, with an active layer depth of
558 79.5 ± 13.7 cm measured in September. The water table in the peat plateau followed the
559 deepening of the seasonally thawed layer.

560 Soil temperatures followed the seasonal climate but were dampened and had temporal
561 lags in deeper peat layers (Figure S1a). The highest young bog and mature bog soil
562 temperatures at 10 cm depth occurred in July, at 14.3 and 14.1 °C, respectively. At 100 cm
563 depth the maximum temperatures occurred in August and September, at 8.6 and 6.9 °C,
564 respectively for the young and mature bog. Soil temperatures at 250 cm were still rising at the
565 end of September, peaking at 4.1 and 3.2 °C in the young bog and mature, respectively. The
566 young bog was consistently warmer than the mature bog throughout the study by on average
567 0.9 ± 0.9 °C, 1.8 ± 1.0 °C, and 0.5 ± 0.4 °C at 10 cm, 100 cm, and 250 cm depths,
568 respectively.

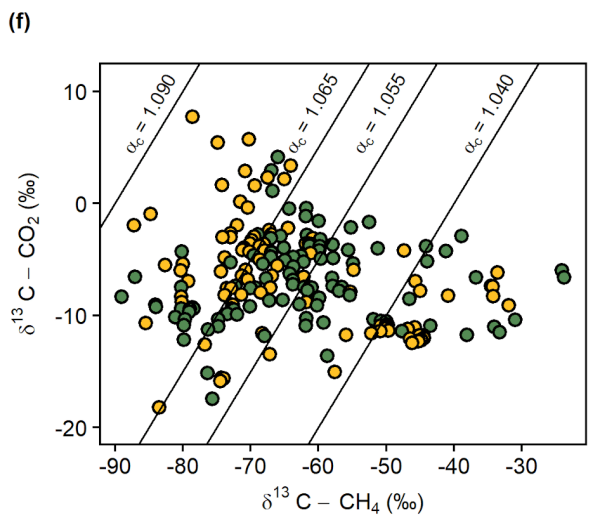
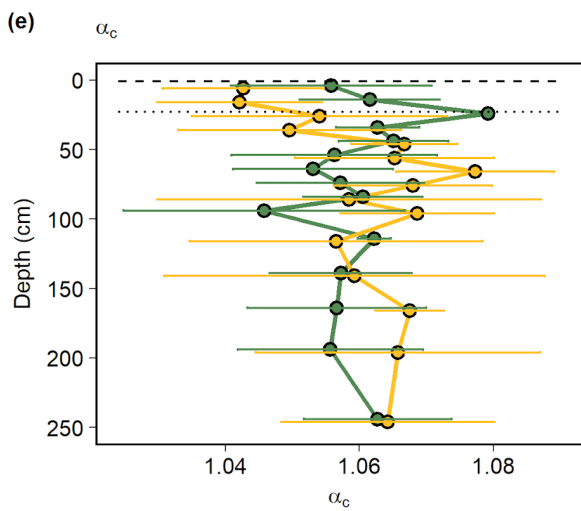
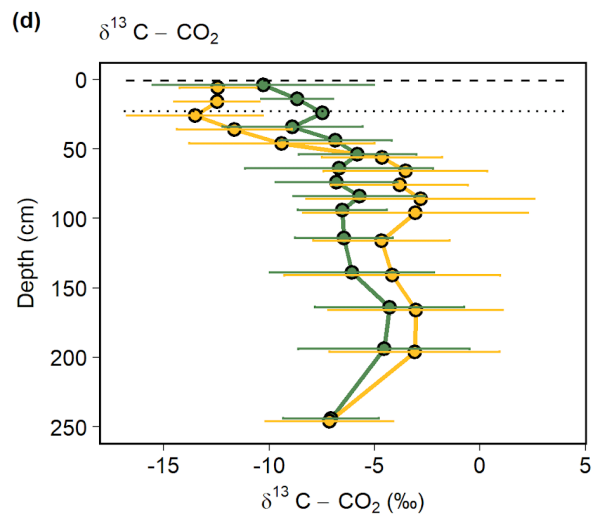
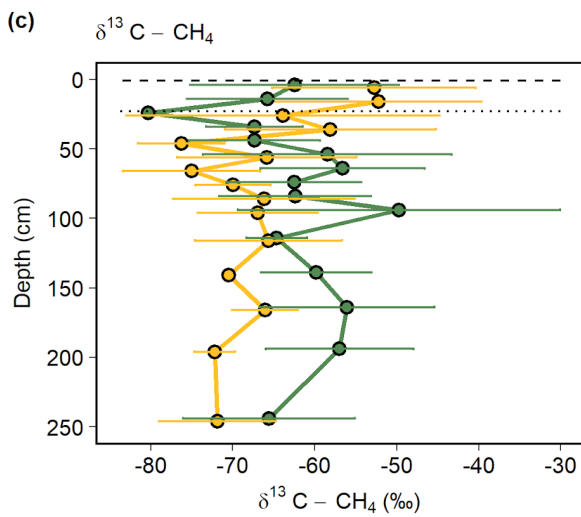
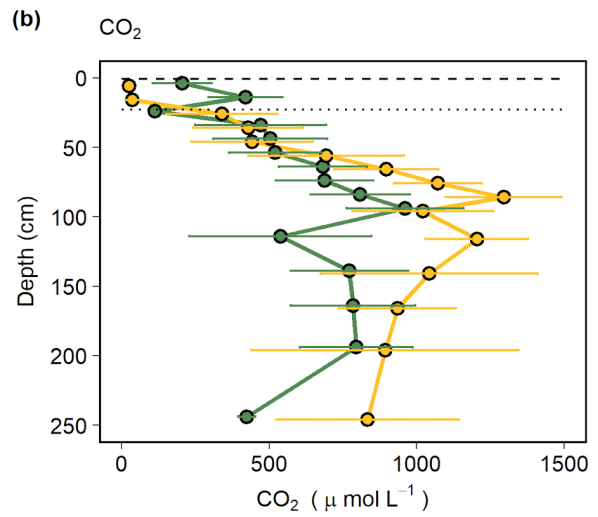
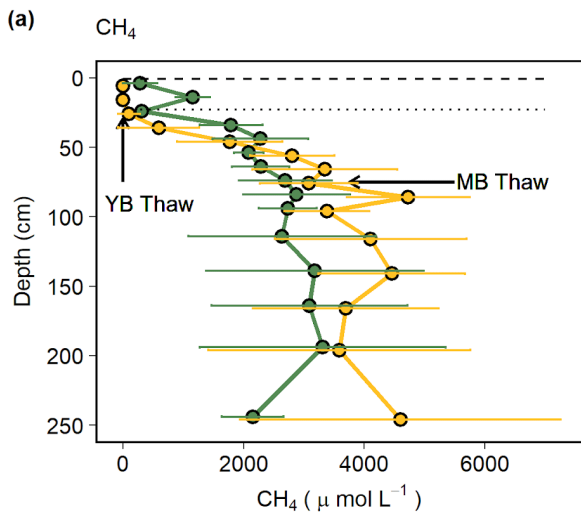
569 Across all depths and sampling occasions, average pH was higher (ANOVA: $F_{(1, 77)} = 35.2, P < 0.001$) in the young bog than in the mature bog at 4.1 ± 0.2 and 3.9 ± 0.2
570 respectively. In contrast, DOC at 69.2 ± 18.4 and 53.8 ± 5.4 mg C L⁻¹ (ANOVA: $F_{(1, 82)} = 38.7, P < 0.001$) and total dissolved nitrogen at 1.5 ± 1.4 and 0.9 ± 0.1 mg L⁻¹ (ANOVA: $F_{(1, 82)} = 12.8, P < 0.01$) were higher in the mature bog than in the young bog, respectively.
571 Average SUVA was also higher in the young bog (3.2 ± 0.4 L mg C⁻¹ m⁻¹) compared to the
572 mature bog (2.6 ± 0.4 L mg C⁻¹ m⁻¹), indicating DOM with a greater aromatic content in the
573 young bog. In contrast, DOC (69.2 ± 18.4 and 53.8 ± 5.4 mg C L⁻¹) and total dissolved
574 nitrogen (1.5 ± 1.4 and 0.9 ± 0.1 mg L⁻¹) were higher in the mature bog than in the young
575 nitrogen (1.5 ± 1.4 and 0.9 ± 0.1 mg L⁻¹) were higher in the mature bog than in the young
576 nitrogen (1.5 ± 1.4 and 0.9 ± 0.1 mg L⁻¹) were higher in the mature bog than in the young
577 nitrogen (1.5 ± 1.4 and 0.9 ± 0.1 mg L⁻¹) were higher in the mature bog than in the young

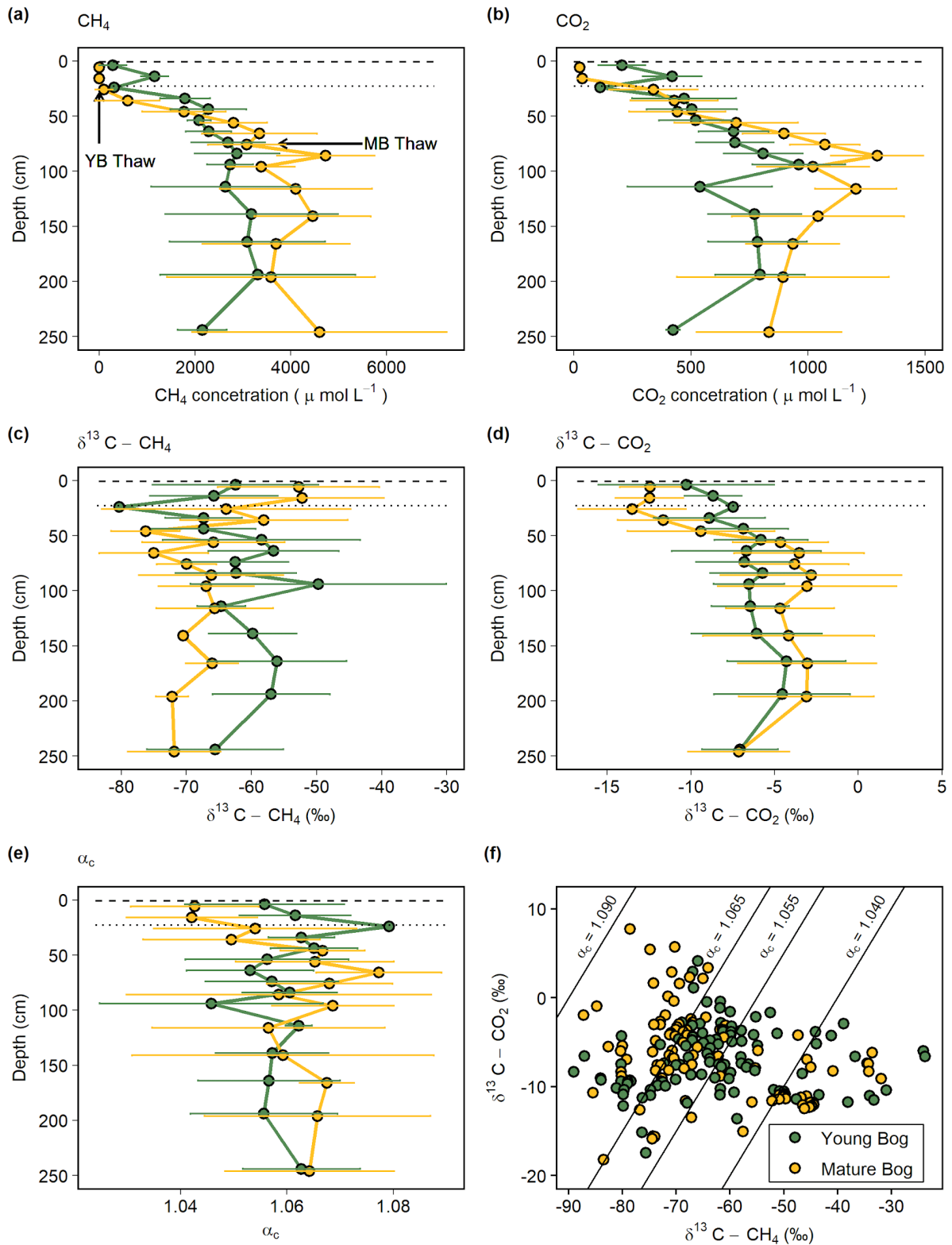
578 ~~bog, respectively.~~ Average SUVA values were higher (ANOVA: $F_{(1, 82)} = 103.5, P < 0.001$)
579 in the young bog ($3.2 \pm 0.4 \text{ L mg C}^{-1} \text{ m}^{-1}$) compared to the mature bog ($2.6 \pm 0.4 \text{ L mg C}^{-1} \text{ m}^{-1}$),
580 indicating DOM with a greater aromatic content in the young bog. However, average
581 spectral slope ($S_{250-465}$) values were also greater (ANOVA: $F_{(1, 81)} = 6.9, P < 0.05$) in the
582 young bog ($-0.016 \pm 0.002 \text{ nm}^{-1}$) compared to the mature bog ($-0.017 \pm 0.003 \text{ nm}^{-1}$),
583 indicating lower molecular weight and decreasing aromaticity. Average phenolics (0.6 ± 0.2
584 and $0.6 \pm 0.2 \text{ mg L}^{-1}$), ~~spectral slope ($S_{250-465}$: -0.016 ± 0.002 and $-0.017 \pm 0.003 \text{ nm}^{-1}$),~~ and
585 phosphate (PO_4^{3-} : 9.0 ± 14.3 and $6.7 \pm 3.0 \text{ } \mu\text{g L}^{-1}$) were similar between the young bog and
586 mature bog, respectively, across all depths and sampling occasions. Full details of DOM
587 chemistry results can be found in Heffernan et al., (2021). Of note is the fact that the pore
588 water chemistry was compared across all depths in this study, in contrast to Heffernan et al.,
589 (2021) in which pore water found above and below the transition indicating permafrost thaw
590 was compared.

591 *3.2 Concentrations and isotopic signatures of dissolved gases*

592 Dissolved CH_4 increased with depth ~~under~~ below the water table in both the young
593 and mature bog (Figure 2a). ~~Concentrations~~ Dissolved CH_4 concentrations of CH_4 in the
594 young bog increased with depth, from $-19 \text{ } \mu\text{mol L}^{-1}$ at 5 cm depth, to a peak of $5,400 \text{ } \mu\text{mol L}^{-1}$
595 at 195 cm. Dissolved CH_4 concentrations ~~Concentrations of CH_4~~ in the mature bog remained
596 low above the water table ($<6 \text{ } \mu\text{mol L}^{-1}$ below 25 cm), but then increased to $4,100 \pm 1,700$
597 $\text{ } \mu\text{mol L}^{-1}$ between 115 and 250 cm depth and peaked at $6,800 \text{ } \mu\text{mol L}^{-1}$. Dissolved CO_2
598 concentrations followed a very similar pattern to CH_4 , increasing with depth in both the
599 young and mature bog (Figure 2b). Again, the mature bog had overall higher concentrations,
600 with mean average values ranging from $340 - 1,295 \text{ } \mu\text{mol L}^{-1}$ and peaking at $1,500 \text{ } \mu\text{mol L}^{-1}$

601 at 85 cm. ~~while~~ Whereas in the young bog average values ranged from 113 – 960 $\mu\text{mol L}^{-1}$
602 and peaked at 1,200 $\mu\text{mol L}^{-1}$ at 95 cm (Figure 2b).





605

606 **Figure 2.** Average seasonal (May – September) depth profiles in the young (green, black
 607 circles) and mature (yellow, black circles) bog of (a) dissolved CH₄ concentration ($\mu\text{mol L}^{-1}$),
 608 (b) dissolved CO₂ concentration ($\mu\text{mol L}^{-1}$), (c) $\delta^{13}\text{C}-\text{CH}_4$ (‰), (d) $\delta^{13}\text{C}-\text{CO}_2$ (‰), and (e)
 609 apparent fractionation factor (α_c) between dissolved CH₄ and CO₂. (f) Cross-plot of
 610 corresponding $\delta^{13}\text{C}-\text{CH}_4$ and $\delta^{13}\text{C}-\text{CO}_2$ values (‰) in the young bog and mature bog, from

611 raw data used in panels (c) and (d). Diagonal lines represent different α_c where α_c 1.040 –
612 1.065 represents acetoclastic methanogenesis, and α_c 1.055 – 1.09 represents
613 hydrogenotrophic methanogenesis (Whiticar, 1999). (a) – (e) Dashed and dotted horizontal
614 lines represent water table depth in the young (YB) and mature bog (MB) respectively.
615 Arrows in panel (a) represent depth of thaw transition in both the young (29 cm) and mature
616 bog (71 cm), i.e., the transition from deep peat (accumulated prior to thawing) and shallow
617 peat (accumulated post thawing).

618

619 The young bog and mature bog had distinct profiles of $\delta^{13}\text{C}$ isotopic signatures values for
620 both CH_4 and CO_2 (Figure 2c, d). The young bog had no apparent trend ~~in~~ with depth for both
621 $\delta^{13}\text{C}\text{-CH}_4$ ~~by depth~~ (ANOVA: $F_{(14, 45)} = 1.75, P = 0.08$) and $\delta^{13}\text{C}\text{-CO}_2$ (ANOVA: $F_{(14, 46)} =$
622 $1.79, P = 0.07$), averaging $-62.4 \pm 7.0 \text{ ‰}$ and $-6.8 \pm 1.6 \text{ ‰}$, respectively ~~ranging between~~
623 ~~49.7 ‰ and 80.3 ‰~~ (Figure 2c, d). In the mature bog we observed significant depth trends
624 for both isotopically heavy $\delta^{13}\text{C}\text{-CH}_4$ (ANOVA: $F_{(14, 43)} = 3.19, P < 0.01$) and $\delta^{13}\text{C}\text{-CO}_2$
625 (ANOVA: $F_{(14, 49)} = 6.22, P < 0.001$). These significant depth trends are due to isotopically
626 heavy $\delta^{13}\text{C}\text{-CH}_4$ and light $\delta^{13}\text{C}\text{-CO}_2$ above the water table, which suggest ~~ed~~ an influence
627 from CH_4 oxidation. When comparing $\delta^{13}\text{C}$ depth profiles between the thermokarst bogs we
628 focused on those values taken from under the water table to avoid the effect of CH_4 oxidation
629 observed above the water table in the mature bog. Under the water table, $\delta^{13}\text{C}\text{-CH}_4$ values in
630 the mature bog ~~had were~~ significantly lighter (ANOVA: $F_{(1, 64)} = 18.72, P < 0.001$) $\delta^{13}\text{C}\text{-CH}_4$
631 compared to the young bog at an average of $-68.7 \pm 5.0 \text{ ‰}$ and $-62.4 \pm 7.0 \text{ ‰}$, respectively ($F_{(1, 92)} = 17.25, P < 0.001$). ~~In the young bog, $\delta^{13}\text{C}\text{-CO}_2$ had no apparent trend with depth~~
632 ~~(average $-6.8 \pm 1.6 \text{ ‰}$).~~ The Conversely, the mature bog had isotopically lighter $\delta^{13}\text{C}\text{-CO}_2$
633 ~~above the water table and was isotopically~~ heavier $\delta^{13}\text{C}\text{-CO}_2$ than the young bog below the
634 water table (ANOVA: $F_{(1, 9971)} = 5.3313.86, P < 0.05001$).

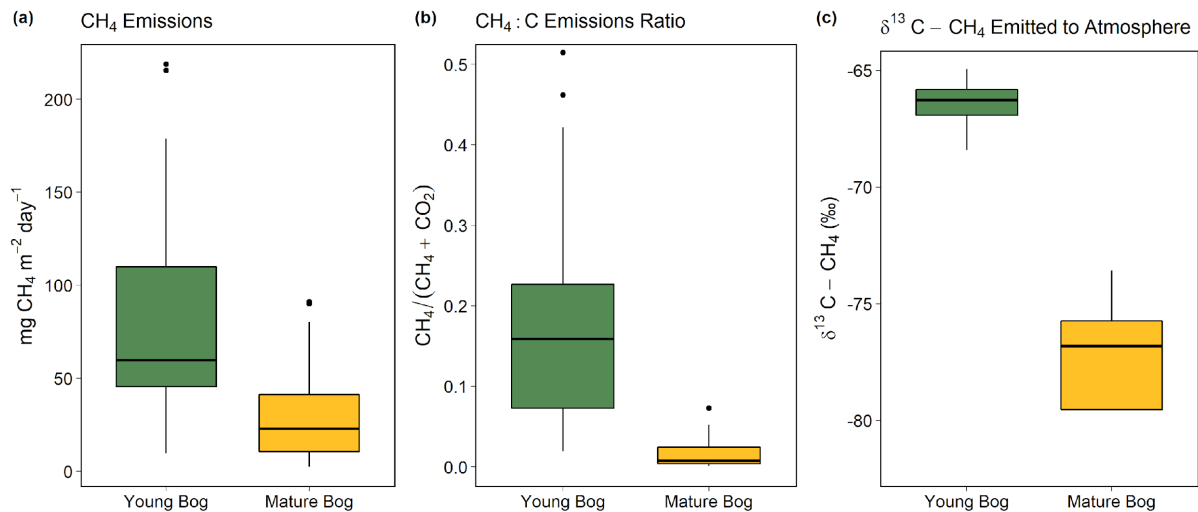
636 The apparent fractionation factor (α_c) is a robust parameter to characterize the relative
637 contribution of CH_4 production pathways, with values of 1.040 – 1.060 indicating
638 acetoclastic methanogenesis and 1.060 – 1.090 for hydrogenotrophic methanogenesis

639 (Chanton et al., 2005). Similar to the gas $\delta^{13}\text{C}$ depth-profiles, we found no clear trend with
640 depth in for α_C values with depth in the young bog (ANOVA; $F_{(14, 44)} = 0.87, P = 0.59$) with
641 an average of 1.058 ± 0.012 and range of 1.018 – 1.079 (Figure 2e). In the mature bog, we
642 found a clear depth trend in α_C values (ANOVA: $F_{(14, 43)} = 5.71, P < 0.001$). Similar to the
643 $\delta^{13}\text{C}$ depth profiles in the mature bog, this significant depth trend the average in α_C was lowest
644 in samples collected above the water table at 5, 15, and 25 cm, likely is due to the influence
645 of CH_4 oxidation above the water table, with the lowest α_C values being those from samples
646 collected above the water table at 5, 15, and 25 cm. The average α_C beneath the water table in
647 the mature bog was 1.064 ± 0.017 and ranged from 1.015 – 1.094. When comparing α_C values
648 from beneath the water table between the young and mature bog, we found that α_C values
649 were significantly lower in similar to the average values found in the young bog (ANOVA: $F_{(1, 9963)} = 0.730.8, P = < 0.4001$).
650

651 In the isotopic ratio cross-plot of $\delta^{13}\text{C}\text{-CH}_4$ and $\delta^{13}\text{C}\text{-CO}_2$ (Figure 2f), most of the young
652 bog had α_C values of between 1.055 – 1.065 (29 in total), with a greater number of samples
653 (21) between $\alpha_C = 1.040$ – 1.055, compared to the mature bog (15). In contrast, a greater
654 proportion of the mature bog samples had $\alpha_C > 1.065$ (42 in the young bog and 52 in the
655 mature bog). There was no clear depth trend in the α_C values and no samples in this study had
656 $\alpha_C > 1.090$. Several samples (13) from the young bog and mature bog had α_C values of <
657 1.040, likely due CH_4 oxidation (Knorr et al., 2009). The $\delta^{13}\text{C}\text{-CH}_4$ signature of CH_4
658 emissions (intercept values from Keeling plots), in the young bog were significantly greater
659 than those observed in the mature bog (Figure 3e; $F_{(1, 4)} = 20.67, P < 0.05$), suggesting a
660 greater influence of acetoclastic CH_4 production. Overall, the isotopic data indicates a general
661 dominance of hydrogenotrophic methanogenesis in both sites, but a greater contribution of
662 acetoclastic methanogenesis in the young bog relative to the mature bog.

663 3.3 Magnitude and isotopic signature of land-atmosphere gas fluxes

664 The young bog had almost three times greater average CH₄ fluxes than the mature bog
665 during the May – September study period, at 82.3 ± 21.9 mg CH₄ m⁻² day⁻¹ and 30.8 ± 10.6
666 mg CH₄ m⁻² day⁻¹, respectively (Figure 3a). Fluxes of CH₄ in the young bog were greatest
667 between June and August, ranging from 80.6 ± 40.3 mg CH₄ m⁻² day⁻¹ to 100.9 ± 63.1 mg
668 CH₄ m⁻² day⁻¹. The lowest young bog CH₄ fluxes were observed in September at 55.0 ± 17.7
669 mg CH₄ m⁻² day⁻¹ (Figure S3a). Mature bog CH₄ fluxes were greatest in September ($55.8 \pm$
670 21.1 mg CH₄ m⁻² day⁻¹) and lowest in May (5.6 ± 2.7 mg CH₄ m⁻² day⁻¹). Ecosystem
671 respiration (CO₂ emissions measured with dark chambers) was significantly lower in the
672 young bog than mature bog, with study period averages of 0.6 ± 0.3 and 1.9 ± 0.3 g CO₂ m⁻²
673 day⁻¹, respectively (Figure S32b). Maximum ecosystem respiration in the young bog occurred
674 in August (1.6 g CO₂ m⁻² day⁻¹) and was much lower during the other four months (monthly
675 averages of 0.2 to 0.4 g CO₂ m⁻² day⁻¹). Maximum ecosystem respiration rates in the mature
676 bog were elevated was found for the period from June to August (monthly averages between
677 2.1 and 2.6 g CO₂ m⁻² day⁻¹), with lower emissions and decreased in September (0.8 g CO₂ m⁻²
678 day⁻¹). The proportion of total C emissions (sum of CH₄ and CO₂ emissions) released as
679 CH₄ were as an order of magnitude greater in the young bog than mature bog stage, at 18
680 and 2% respectively. This, resulting from was a result of both the young bog higher CH₄
681 emissions and lower ecosystem respiration (Figure S3) in the young bog. The δ¹³C-CH₄
682 signature of CH₄ emissions (intercept values from Keeling plots), in the young bog were
683 significantly greater than those observed in the mature bog (Figure 3c; ANOVA: $F_{(1,4)} =$
684 20.67 , $P < 0.05$), suggesting a greater influence of acetoclastic CH₄ production. The average
685 δ¹³C-CH₄ isotopic signature of CH₄ emissions in the young bog CH₄ emissions (n = 4) was -
686 66.5 ± 1.4 ‰ (Figure 3e 95% CI) and 78.5 ± 5.6 ‰ (95% CI; Figure 3c) in the, whereas the
687 average from mature bog emissions (n = 4) was 78.5 ± 5.6 ‰ (95% CI).



688

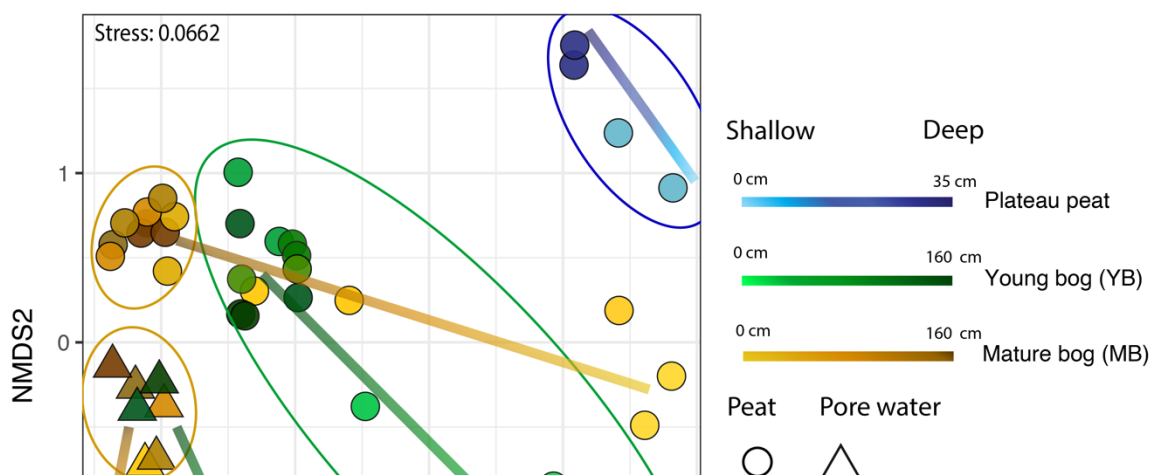
689 **Figure 3.** Magnitude and isotopic signature of greenhouse gas fluxes from the young bog
 690 (green) and mature bog (yellow) shown as boxplots. Boxes represents the interquartile range
 691 (25 – 75%), with median shown as black horizontal line. Whiskers extend to 1.5 times the
 692 interquartile range (distance between first and third quartile) in each direction, with outlier
 693 data plotted individually as black dots (a) The magnitude of net land-atmosphere CH₄
 694 emissions as measured by soil chambers. (b) The ratio between CH₄ emissions and the sum of
 695 CO₂ emissions (ecosystem respiration) and CH₄, both standardized to per g C. (c) Intercept
 696 values of Keeling plots indicating the δ¹³C-CH₄ signature of CH₄ emissions. Isotopically
 697 heavier (i.e., less negative) δ¹³C-CH₄ is produced via acetoclastic methanogenesis, whereas
 698 isotopically lighter (i.e., more negative) δ¹³C-CH₄ is produced via hydrogenotrophic
 699 methanogenesis. The CH₄ and CO₂ land-atmosphere fluxes shown in (a) and (b) were
 700 measured once a month from May – September 2018. The δ¹³C-CH₄ of CH₄ emitted to the
 701 atmosphere was measured in September and October 2016 (see methods for details and
 702 Figure S4 for Keeling plots).

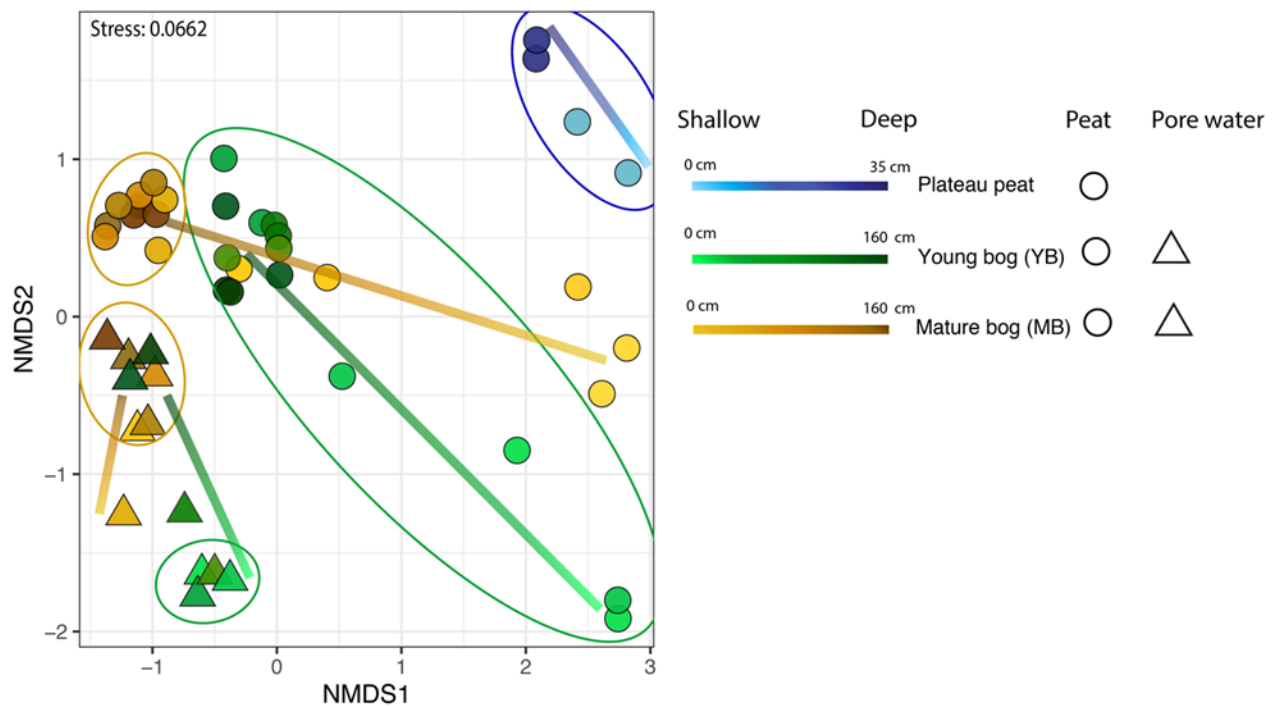
703

704 3.4 Microbial community structure along the permafrost peatland thaw gradient

705 We used NMDS ordinations to assess differences in microbial community structure
 706 between solid peat and pore water samples, between sampling depths, and between the
 707 plateau, young bog, and mature bog. The only exception was the plateau, where only peat
 708 samples were collected (i.e., no pore water samples). Microbial community structure in
 709 peat was determined to be significantly different from porewater microbial communities
 710 (PERMANOVA, $R^2 = 0.13$, $P < 0.05$, Figure 4). The differences observed in the microbial
 711 community structure between peat and pore water samples could be a function of the

712 different extraction methods used to extract DNA (Carrigg et al., 2007). Among the pore
 713 water samples, distinct microbial communities were found to be associated with the young
 714 bog and mature bog. Similarly, microbial community structure in peat was found to be
 715 significantly distinct between the three successional stages (plateau peat, young bog and
 716 mature bog; Figure 4; PERMANOVA, $R^2 = 0.18$, $P < 0.05$). There is also a common trend
 717 in vertical community structuring for all sample matrices according to depth. Changes in
 718 overall microbial community composition in both peat and pore water, across a vertical
 719 profile (to a maximum depth of 160 cm), illustrate a confluence in microbial community
 720 structure with depth in both the young and mature bog (Figure 4). In other words, community
 721 structure was most dissimilar at depths closer to the surface (Figure 4, Figure S2b, c;
 722 PERMANOVA; $R^2 = 0.16$, $P < 0.05$). This trend was particularly evident in the porewater
 723 samples (Figure 4). In the peat samples, though microbial communities did not fully
 724 converge, deeper young bog peat (i.e., 90 – 160 cm) communities did become more similar to
 725 communities found in the mature bog at intermediate depths (i.e., 30 – 70 cm), based on the
 726 nearness of sample points on the NMDS (Figure 4). We also observed that the mature bog
 727 near-surface peat samples were located closer to the plateau peat on the NMDS (Figure 4,
 728 PERMANOVA; $R^2 = 0.4$, $P = 0.2661$). It was not possible to assess the presence of this
 729 cyclic succession (from young bog to mature bog to plateau) in the pore water samples since
 730 we did not characterize the microbial community in the plateau pore water. Finally, we also
 731 assessed the effect of seasonality on microbial community ~~structure diversity~~ and found no
 732 effect with regards to sampling month (PERMANOVAANOSIM; $R^2 = 0.02$, $P = 0.559090$).



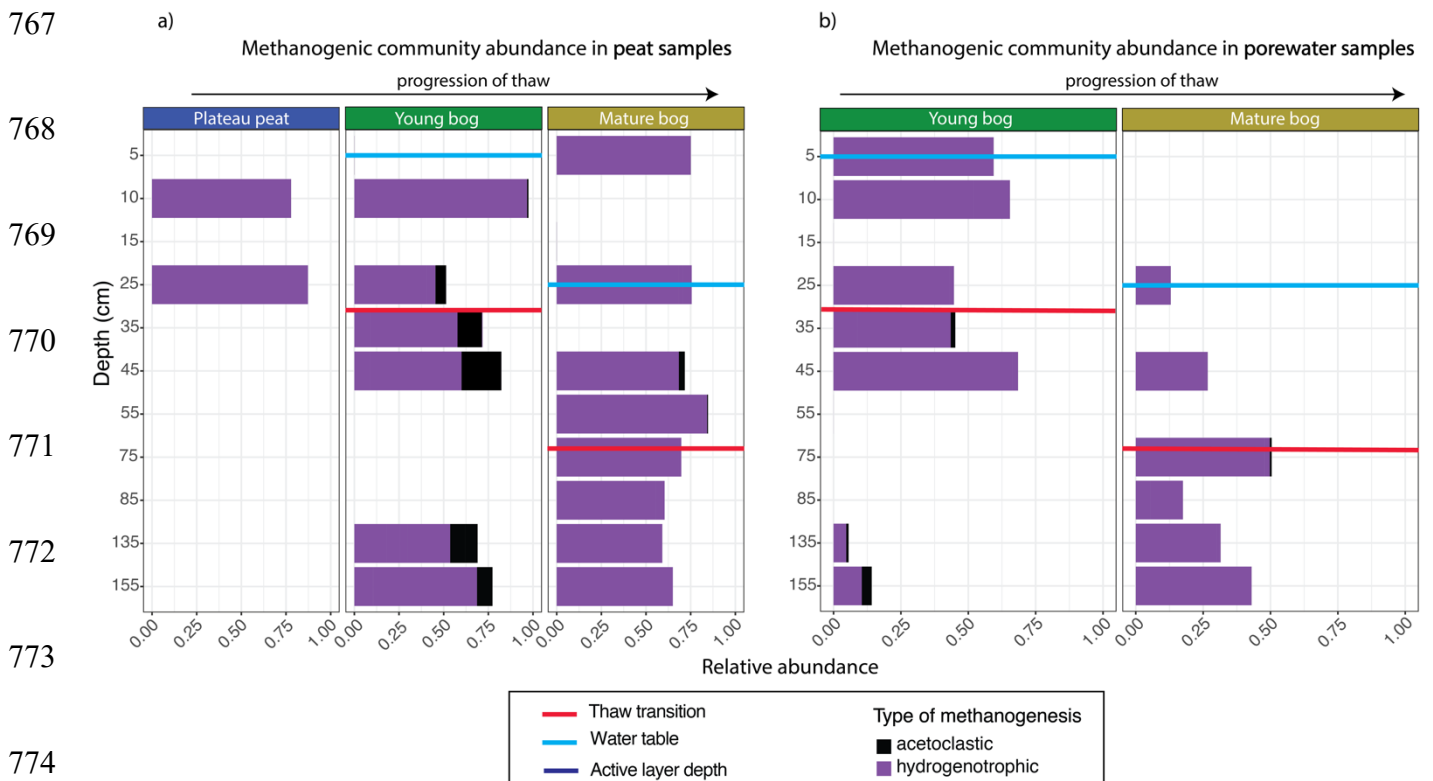


734
735
736
737
738
739
740
741
742
743
744

745 **Figure 4.** Microbial community distribution according to stage of peat/pore water. NMDS
746 ordinations of amplicon sequencing variant (ASV) data demonstrate significant community
747 dissimilarities ([PERMANOVA, \$R^2 = 0.13\$, \$P < 0.05\$](#) ~~PERMANOVA; $P < 0.05$~~) according to
748 thaw stage for both pore water (shown by the triangles) and peat (shown by the circles)
749 samples, encircled by 95% confidence intervals. Colour gradient and lines demonstrate the
750 shift in microbial community structure along vertical depth profiles where lighter shades
751 indicate samples closer to the surface.

752

753 The total archaeal community comprised 6% of the entire microbial dataset.
 754 Methanogen-related orders comprised 54% of this archaeal dataset and demonstrated marked
 755 differences in the relative abundance of acetoclastic-related methanogens according to thaw
 756 stage and depth in both peat and pore water samples (Figure 5; Figure S2). In the young and
 757 mature bog peat samples, hydrogenotrophic-related methanogens were ubiquitously present
 758 throughout both depth profiles (Figure 5a). In comparison, acetoclastic-related methanogens
 759 exhibited a relatively restricted presence, only present at specific depths (Figure 5a). These
 760 communities were most abundant (>25% of the total methanogenic community) near the
 761 surface in the young bog, just above and below the thaw transition zone (Figure 5a). In the
 762 pore water, hydrogenotrophic methanogens were also dominant throughout depths in both
 763 stages of thaw (Figure 5b). However, in contrast to peat samples, acetoclastic methanogens
 764 were virtually absent in the pore water, although minimally present (i.e., $\leq 10\%$ relative
 765 abundance) at depths between 35 and 155 cm, all found below the thaw transition zone
 766 (Figure 5b).



775

776 **Figure 5.** Relative abundance of archaeal orders according to putative methanogenic
777 capability, along a depth profile for peat and pore water samples. Samples are arranged
778 according to depth (y axis), with the relative abundance of methanogenic archaea resolved
779 shown on the x axis. Note that the y axis does not uniformly progress in 10 cm increments.
780 Progression of thaw is shown from plateau peat to young bog to mature bog at the top of the
781 figures, with position of water table shown in blue for each panel. Red lines demonstrate
782 thaw transition zone for the young bog and mature bog. (a) Stacked bar plot of methanogenic
783 Archaea for all peat samples. Samples demonstrate significant differences in putative
784 methanogen composition between all stages (Kruskall-Wallis test & Wilcox rank sum test,
785 with Benjamini-Hochberg corrected p-values, $P < 0.05$). (b) Stacked bar plot of
786 methanogenic Archaea for all pore water samples. Samples do not demonstrate significant
787 differences in putative methanogen composition between stages (Kruskall-Wallis test, with
788 Benjamini-Hochberg corrected p-values, $P = 0.965$).

789

790 Using a redundancy analysis (RDA, Figure 6) we found that 27.6% of variation in the

791 methanogenic community was explained by two variables: thaw stage (ANOVA, $P < 0.05$)

792 and depth from the water table (ANOVA, $P < 0.05$). [Although these were the only two](#)

793 [parameters that were identified as significant variables impacting microbial community](#)

794 [structure when using a backward stepping model, it should be noted that there may be more](#)

795 [variation in the community that our experimental design does not take into account as a result](#)

796 [of unconstrained variation represented by plant-microbe and/or microbe-microbe interactions](#)

797 [\(Boon et al., 2014\). Nonetheless, the 27.6% variation explained](#) is in accordance with other

798 studies conducted in permafrost impacted regions using similar methods, where the

799 ~~percentage of~~ [percentage of](#) explained variation falls between -6% (low) to 43% (high)

800 (Comte et al., 2015; Hough et al., 2020). Next, we used variance partitioning to assess the

801 extent to which thaw stage and depth from the water table (~~i.e.~~ [i.e.](#), the significant

802 environmental variables identified by the RDA) explained the variation in only the

803 methanogenic community structure (Figure 6). Based on this analysis, thaw stage explained

804 18.4% and distance to the water table explained 4.3% of methanogenic community variation,

805 respectively.

806

807
808
809
810
811
812
813
814
815
816
817
818
819
820
821
822
823
824
825
826
827
828
829
830
831
832
833
834
835
836
837
838
839
840

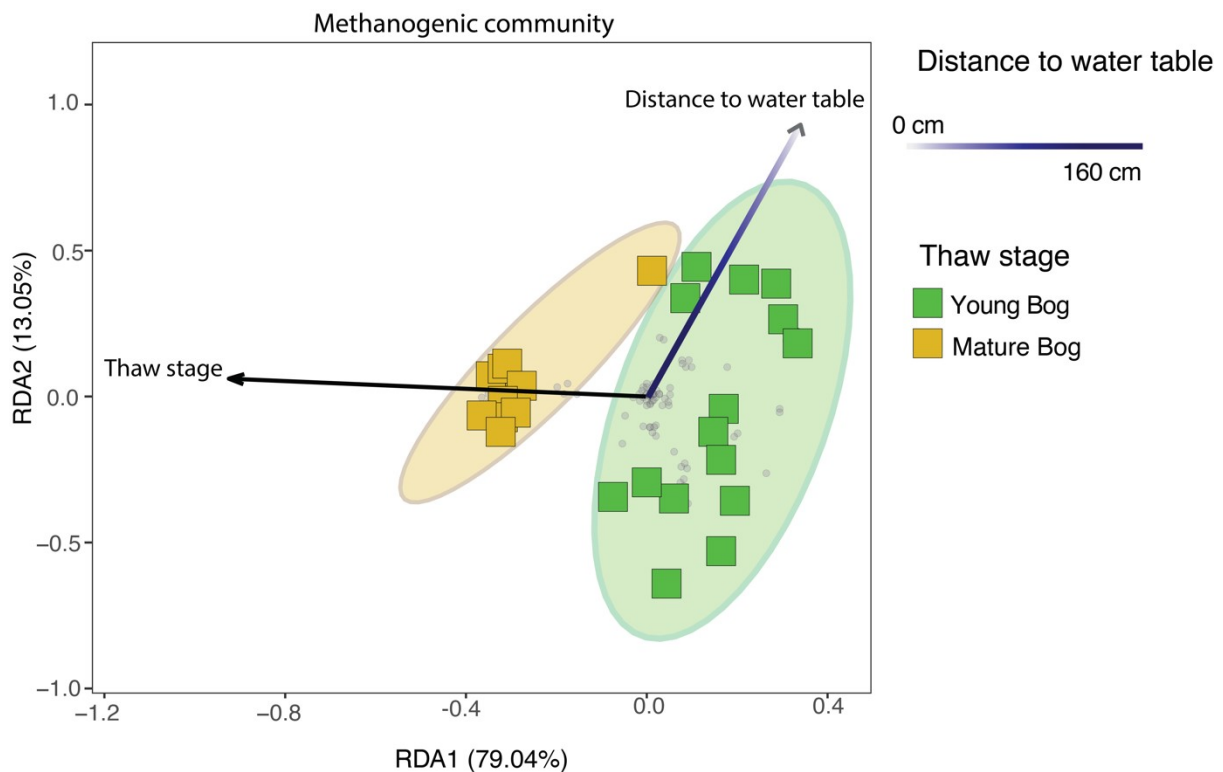


Figure 6. Redundancy analysis (RDA) exploring biotiesignificant biotic and abiotic variables influencing the total methanogenic community (adjusted $R^2 = 27.6\%$), as determined by a backward stepping RDA model in the peat and pore water samples. All parameters that were used in model are described in section 2.10 of the Methods. Grey dots in the panel demonstrate the distribution of all ASVs in the methanogenic dataset. Shaded ellipses represent the 95% confidence intervals for microbial community structure-diversity according to peatland thaw stage (young bog vs mature bog). Only significant (ANOVA, $P < 0.05$) variables are shown. Using variation partitioning, we found that peatland thaw stage significantly explains about 18.4% of methanogenic community variation whereas distance to water table explained 4.3%. Both axes are significant (ANOVA, $P < 0.05$).

4. Discussion

Our study shows that high CH_4 emissions from thermokarst bogs in the initial decades following permafrost thaw (young bog) are not only linked to environmental conditions (wetness, soil temperature, vegetation), but also driven by relatively increased microbial CH_4 production through the energetically more favourable acetoclastic methanogenesis pathway.

841 Evidence of acetoclastic methanogens and CH₄ produced via the acetoclastic metabolic
842 pathway was found in the young bog both near the surface and at depths below the thaw
843 transition (i.e., in peat that accumulated prior to permafrost thaw). We are unable to
844 determine whether these greater CH₄ emissions in the initial decades following thaw are due
845 to the mineralization of labile organic matter released from previously frozen peat, or are
846 driven solely by fresh, labile DOM derived from surface vegetation leached throughout the
847 peat profile. [However, previous work in the discontinuous permafrost region in the Interior
848 Plains of western Canada has found a limited contribution of previously frozen organic
849 matter contributing to surface CH₄ emissions in thermokarst bogs \(Cooper et al., 2017\).](#)
850 Elevated CH₄ emissions then slow over the following centuries with succession into a mature
851 thermokarst bog stage where CH₄ production is almost exclusively through the
852 hydrogenotrophic pathway.

853 *4.1 Shift in microbial community assemblages along a permafrost thaw gradient*

854 Microbial communities varied along the permafrost thaw gradient; among different thaw
855 stages (permafrost peat plateau, young bog, and mature bog), with peat depth (surface down
856 to 160 cm), and between different sample types (solid peat and pore water). We found clear
857 differences in microbial communities between the young bog and mature bog, despite similar
858 peat stratigraphy up to the surficial vegetation (Heffernan et al., 2020), where dominant
859 *Sphagnum* species varied. The greater height of the peat surface above the water table and
860 [relatively](#) drier conditions in the mature bog, due to the slow accumulation of new peat over
861 centuries, leads to a shift in vegetation composition from hydrophilic *Sphagnum* and
862 graminoids towards more drought resistant *Sphagnum* spp. and ericaceous shrubs. This shift
863 in water table position and vegetation community, along with a decrease in temperatures
864 (Figure S1a) due to the thermal insulating properties of *Sphagnum* peat (Kujala, Seppälä, &

865 Holappa, 2008) appears to have caused the observed differences in microbial communities
866 between the young and mature bog, even at depths >1 m. Microbial communities were most
867 dissimilar between the peat plateau and young bog. This was unsurprising given the abrupt
868 shift from the elevated, frozen, and relatively dry peat plateau forest to the young bog where
869 the surface was saturated, dominated by hydrophilic vegetation and had warmer
870 temperatures. We further noted that the microbial community of the mature bog was more
871 similar with the peat plateau than with the young bog. Paleo-records in the region (Heffernan
872 et al., 2020; Pelletier et al., 2017; Zoltai, 1993) show that many peatlands have undergone
873 cyclical permafrost developments, as thermal insulating properties of *Sphagnum* peat in
874 mature bogs leads to the re-aggradation of permafrost peat plateaus. Our study suggests that
875 the peat plateau microbial community is influenced by the preceding mature bog microbial
876 community as permafrost aggrades.

877 The most dissimilar microbial community composition was observed between
878 samples near the surface and those at depth (i.e., down to 160 cm), as has [also been also](#)
879 observed in other permafrost ecosystems (Frey et al., 2016; Monteux et al., 2018). Shifts in
880 microbial community composition along the thaw gradient were most evident nearer the
881 surface, whereas communities found at depth were similar between the young bog and mature
882 bog (Figure 4). At the surface, microbial community structure is influenced by the
883 successional vegetation community (Hodgkins et al., 2014) and the role that vegetation,
884 [particularly graminoids which are found in the young bog,](#) has on microbial community
885 structure has been well documented in northern peatlands (Robroek et al., 2015, 2021;
886 [Bragazza et al., 2015](#)). [Moderately acidic, saturated peatlands with hydrophilic vegetation,](#)
887 [similar to the young bog, have been shown to harbour acid tolerant fermenting bacteria that](#)
888 [produce substrates for methanogenesis and are trophically linked with methanogens \(Wüst et](#)
889 [al., 2009\).](#) Thus, the interaction between water table position, pH, and vegetation community

890 [influences the substrates available to the microbial community, which in turn impacts the](#)
891 [surface community's structure \(Kotiaho et al., 2013\).](#) In contrast, communities at depth are
892 known to be influenced by peat properties, such as peat chemistry and degree of
893 decomposition, and the paleoenvironment under which they originally colonized (Lee et al.,
894 2012; Holm et al., 2020). In the young and mature bog both peat properties (humification
895 indices including FTIR 1630/1090 cm^{-3} and C:N ratios) and the paleoenvironment at depth
896 are similar (Heffernan et al., 2020), which may explain the observed convergence of
897 microbial community structure. Nonetheless, although there are some similarities at depth
898 between both young and mature bog, microbial communities inhabiting either are still distinct
899 (Figure 4). This is emphasized by the differing abundance of Archaea that participate in
900 hydrogenotrophic or acetoclastic methanogenesis (Figure 5) in both stages down the peat
901 profile.

902 [As has been shown previously in other thermokarst peatlands \(McCalley et al., 2014\),](#)
903 [the young and mature bog stages were dominated by hydrogenotrophic methanogens.](#)
904 [However, acetoclastic methanogens were relatively more abundant in the young bog \(Figure](#)
905 [5\), particularly at or below the transition in peat that accumulated prior to permafrost thaw.](#)
906 [Thaw stage and distance from the water table were found to influence the methanogenic](#)
907 [community composition \(Figure 6\), with distance from the water table dictating where anoxic](#)
908 [conditions persist \(Blodau et al., 2004\) and thus where methanogenic colonization can occur.](#)
909 [The influence of vegetation communities associated with different thermokarst peatland](#)
910 [stages on methanogenic community composition has previously been attributed to the role of](#)
911 [plant derived DOM serving as the substrate for \$\text{CH}_4\$ production \(Liebner et al., 2015;](#)
912 [McCalley et al., 2014\).](#) The presence of hydrophilic vegetation, particularly graminoids, in
913 [the saturated young bog provides the precursors for fermentation, yielding acetate \(Liebner et](#)
914 [al., 2015; Ström et al., 2003, 2012, 2015\) and serving as the substrate for acetoclastic \$\text{CH}_4\$](#)

915 production. The downward transport from the surface of plant derived DOM in the young
916 bog (Chanton et al., 2008) likely provides sufficient acetate for the establishment of
917 acetoclastic methanogens at depth in this environment.

918 ~~As has been shown previously in other thermokarst peatlands (McCalley et al., 2014),~~
919 ~~the young and mature bog stages were dominated by hydrogenotrophic methanogens.~~
920 ~~However, acetoclastic methanogens were relatively more abundant in the young bog (Figure~~
921 ~~5), particularly at or below the transition into peat that accumulated prior to permafrost thaw.~~
922 ~~Thaw stage and distance from the water table were found to influence the methanogenic~~
923 ~~community composition (Figure 6), with distance from the water table dictating where anoxic~~
924 ~~conditions persist (Blodau et al., 2004) and thus where methanogenic colonization can occur.~~
925 ~~The influence of vegetation communities associated with different thermokarst peatland~~
926 ~~stages on methanogenic community composition has previously been attributed to the role of~~
927 ~~plant derived DOM serving as the substrate for CH₄ production (Liebner et al., 2015;~~
928 ~~McCalley et al., 2014). The presence of hydrophilic vegetation, particularly graminoids, in~~
929 ~~the saturated young bog provides the precursors for fermentation, yielding acetate (Strom et~~
930 ~~al., 2003; Strom et al., 2012; Liebner et al., 2015; Strom et al., 2015) and serving as the~~
931 ~~substrate for acetoclastic CH₄ production. The downward transport from the surface of labile,~~
932 ~~plant derived DOM in the young bog (Chanton et al., 2008) likely provides sufficient acetate~~
933 ~~for the establishment of acetoclastic methanogens at depth in this environment.~~

934 *4.2 Production and emissions of CH₄ along a peatland thaw gradient*

935 Isotopic signatures ($\delta^{13}\text{C}$) of dissolved CO₂ and CH₄ and α_{C} values in porewater and
936 the of $\delta^{13}\text{C}$ signature of CH₄ emitted to the atmosphere provided further evidence of
937 relatively elevated acetoclastic methanogenesis in the young bog stage. The general increase
938 in $\delta^{13}\text{C}$ -CO₂ with depth observed at both sites (Figure 2d) indicates accumulation of

939 isotopically heavier $\delta^{13}\text{C-CO}_2$ which is likely explained by the preferential use of isotopically
940 lighter $\delta^{13}\text{C-CO}_2$ during hydrogenotrophic methanogenesis (Hornibrook et al., 2000). As a
941 result, CH_4 tends to become lighter with depth and this was particularly apparent in the
942 mature bog (Figure 2c). This leads to the average α_C values of 1.064 ($\delta^{13}\text{C-CH}_4$; -68.7‰) in
943 the mature bog, which were significantly higher than the 1.058 ($\delta^{13}\text{C-CH}_4$; -62.4‰) observed
944 in the young. Together, the $\delta^{13}\text{C-CH}_4$ and $\delta^{13}\text{C-CO}_2$ data and the resulting α_C depth profiles
945 suggest that the majority of CH_4 is produced via the hydrogenotrophic methanogenic
946 pathway, which supports the findings of the microbial community analysis (Figure 5). Our
947 isotope data also suggests that a greater proportion of CH_4 is produced via acetoclastic
948 methanogenesis throughout the profile in the young bog compared to the mature bog (Figure
949 2c – f). This is evident from lower average α_C values found in the young bog compared to the
950 mature bog, and greater number of these young bog α_C values falling between 1.040 – 1.065
951 which represents acetoclastic methanogenesis (Whiticar, 1999). ~~which~~ These findings again
952 agrees with the relatively greater abundance of acetoclastic methanogens observed at that site
953 (Figure 5).

954 In this study we found that average CH_4 emissions in the initial decades following thaw,
955 in the young bog stage, were 2.5 – 3 times greater than emissions measured in the mature bog
956 stage which had thawed ~200 years ago (Figure 3a). Furthermore, the proportion of CH_4 to
957 overall C emissions (Figure 3b) was considerably greater in the young bog than in the mature
958 bog. In the mature bog the lower water table position leads to both increased CO_2 emissions
959 and decreased CH_4 emissions, resulting in a reduced fraction of C emissions as CH_4 . Previous
960 studies have shown similarly increased CH_4 emissions in the initial decades following thaw
961 (Johnston et al., 2014; Wickland et al., 2006). While our pore water chemistry data is
962 inconclusive with regards to organic carbon characteristics, other work in thermokarst bogs in
963 the Interior Plains of western Canada has shown that the organic matter derived from the

964 [young bog vegetation community is highly labile \(Burd et al., 2020\). Previous work at our](#)
965 [study site has shown that the vegetation community in the young bog is associated with](#)
966 [greater potential enzymatic degradation of organic matter \(Heffernan et al., 2021\). Hydrolysis](#)
967 [of plant derived organic matter by extracellular enzymes leads to the formation of monomers](#)
968 [\(Kotsyurbenko, 2005\). These monomers can be further degraded to form acetate and other](#)
969 [percussors for methanogenesis when present with anaerobic fermenting bacteria \(Hamberger](#)
970 [et al., 2008\) and near the surface and vegetation inputs \(Hädrich et al., 2012\).](#) Our study
971 shows that these higher CH₄ emissions are likely linked to increased wetness, temperatures,
972 and [a vegetation community associated with](#) more labile organic matter which favour a
973 greater proportion of CH₄ produced via acetoclastic methanogenesis, as shown by our δ¹³C-
974 CH₄, α_c depth profiles and microbial community composition analyses.

975 Many factors, including environmental conditions and microbial community structure
976 likely contribute to the differences in net CH₄ emissions from the young and mature bog
977 (Figure 3a). Methane oxidation has been shown to be an important regulator of post-thaw
978 CH₄ emissions (Perryman et al., 2020) and to result in isotopically heavier (i.e., less negative)
979 δ¹³C-CH₄ and lighter (i.e., more negative) δ¹³C-CO₂ (Whiticar, 1999). Our data suggests the
980 role of CH₄ oxidation was different between sites. Methane oxidation was apparent in the
981 δ¹³C-CH₄ and δ¹³C-CO₂ signatures above the water table in the mature bog but no CH₄
982 oxidation is evident in the young bog (Figure 2c, d). The difference in gas flux δ¹³C
983 signatures (Figure 3c) also suggests a greater prevalence of CH₄ oxidation in the mature bog.

984 [However, increased oxidation above the water table in the mature bog is likely not fully](#)
985 [responsible for the observed differences in CH₄ surface emissions and depth profiles between](#)
986 [the young and mature bog. Lower soil temperatures, a vegetation community associated with](#)
987 [reduced substrate availability, the dominance of hydrogenotrophic methanogenesis](#)
988 [throughout the peat profile, and a deeper water table position all contribute to the lower CH₄](#)

989 ~~production and higher CH₄ oxidation observed in the mature bog. However, the observed~~
990 ~~differences between the young and mature bog CH₄ emissions and depth profiles are likely~~
991 ~~not due solely to increased CH₄ oxidation above the water table in the mature bog. The lower~~
992 ~~CH₄ emissions and greater dominance of hydrogenotrophic methanogenesis in the mature~~
993 ~~bog relative to the young bog presumably arise from lower soil temperatures, a vegetation~~
994 ~~shift and associated reduction in labile C substrates as peat aggrades in the mature bog in~~
995 ~~addition to a deeper water table that contributes both to lower CH₄ production and higher~~
996 ~~potential for CH₄ oxidation. However~~ Nonetheless, using this interdisciplinary approach, we
997 are unable to determine the relative contribution of acetoclastic methanogenesis at each depth
998 to the overall emissions at the surface.

999 Our results, and those of others (Euskirchen et al., 2014; Johnston et al., 2014), have
1000 shown that CH₄ emissions exhibit seasonal variation (Figure S32a, c) ~~& Figure S3eb~~.
1001 However, in contrast to some previous findings (Ebrahimi & Or, 2017), we did not observe a
1002 corresponding seasonal response in the microbial community composition (Figure S23a).
1003 This may be a sampling design effect since our study spanned only two months (June and
1004 September), compounded by the fact that we did not have replicate samples to test the
1005 robustness of this finding. However, other studies have also shown that soil microbial
1006 community growth is not impacted by seasonal variations in temperature (Simon et al., 2020)
1007 and that microbial communities require a longer time scale (years-decades-centuries) to
1008 respond to temperature following thaw (Feng et al., 2020). Our results corroborate these
1009 observations, suggesting a long-term response in the microbial community composition to the
1010 ecological shifts associated with autogenic peatland succession following permafrost thaw.
1011 Autogenic peatland succession following thaw occurs on the decade to century timescale,
1012 shifting from recently thawed to mature thermokarst bogs (Camill, 1999). Both recently
1013 thawed (young) and mature thermokarst bogs have distinct hydrological regimes, vegetation

1014 communities, and peat chemistry. Following thaw, associated changes in vegetation and litter
1015 input alters microbial community composition and activity (Adamczyk et al., 2020;
1016 Kirkwood et al., 2021). Such changes in microbial community structure thus impact CH₄
1017 emissions from thermokarst peatlands. Under predicted climatic warming scenarios
1018 differences in microbial community composition have been shown to be increasingly driven
1019 by seasonally independent variables such as substrate quality and the legacy effects of soil
1020 temperatures (Luláková et al., 2019). This study suggests that the ~~ecological~~
1021 ~~conditions~~environmental conditions required for increased methanogenic activity at depth is
1022 limited to the initial decades following thaw, after which the microbial community structure
1023 changes in response to lowering of the water table, lower soil temperatures and shifts in the
1024 vegetation community.

1025 **5. Conclusion**

1026 This study demonstrates that higher CH₄ emissions in thermokarst bogs in the initial
1027 decades following thaw are driven by shifts in vegetation communities that produce organic
1028 matter inputs of varying lability (Burd et al., 2020) and prevalence of anoxic conditions,
1029 which was associated with an increase of acetoclastic methanogenesis in our site. The
1030 influence of this pathway was apparent at depth throughout the peat profile. With succession
1031 following thaw towards a mature thermokarst bog, a shift in water table position and
1032 vegetation composition seems to reduce the role of acetoclastic methanogenesis pathway.
1033 Previous work at this site (Heffernan et al., 2021) and other thermokarst peatlands in the
1034 discontinuous permafrost zone of boreal western Canada (Burd et al., 2020) have indicated
1035 that the vegetation community found in the initial decades following permafrost thaw is
1036 associated with increased potential enzymatic degradation and biodegradability of organic
1037 matter compared to that found in the mature bog. Average growing season CH₄ emissions

1038 were 2.5 – 3 times greater in the recently thawed young bog. Overall, C emissions in the
1039 young bog contained proportionally more CH₄ than those from the mature bog, due to greater
1040 CH₄ production and also reduced CO₂ emissions. These greater CH₄ emissions in the young
1041 bog are driven by a higher contribution to surface emissions from CH₄ produced throughout
1042 the peat profile by acetoclastic methanogens. The response of the microbial community to
1043 permafrost thaw is tied to the shifting ~~ecological conditions~~environmental conditions
1044 associated with peatland autogenic succession. Warmer and wetter conditions in the initial
1045 decades following thaw, in conjunction with a vegetation community associated with greater
1046 availability of labile plant leachates (Bragazza et al., 2015), provides favourable conditions
1047 for acetoclastic methanogens throughout the peat profile. Given the projected increases in
1048 thermokarst peatland formation (Olefeldt et al., 2016), our study suggests that we can expect
1049 a pulse of CH₄ emissions from current regions of the discontinuous permafrost zone. This
1050 pulse will be driven, in part, by increased acetoclastic methanogenesis from labile substrates
1051 in recently thawed thermokarst peatlands. However, this rapid increase in CH₄ emissions will
1052 only remain at the decadal to century scale as autogenic peatland succession results in
1053 relatively drier mature thermokarst bogs, where lower temperatures and less labile substrate
1054 availability leads to a dominance of hydrogenotrophic methanogenesis.

1055

1056 **Data availability**

1057 All biogeochemical and enzyme datasets generated and analyzed during this study are
1058 available in the UAL Dataverse repository, [<https://doi.org/10.5683/SP3/5TSH9V>]. Microbial
1059 sequences used in this study can be accessed from the NCBI database, using accession
1060 number PRJNA660023.

1061

1062 **Author contributions**

1063 All authors contributed to the conception of the work. LH and CEA performed the field work
1064 component. LH performed the biogeochemistry measurements. MAC performed the
1065 microbial measurements. LH and MAC analyzed the data and wrote the manuscript draft. All
1066 authors reviewed and edited the manuscript.

1067 **Competing interests**

1068 The authors declare that they have no conflict of interest.

1069 **Acknowledgements**

1070 The authors wish to thank McKenzie Kuhn, Maya Frederickson, Jördis Stührenberg, and Trisha
1071 Elliot for assistance with field and lab work. We also thank Sophie Dang, at MBSU for
1072 providing guidance throughout 16S rRNA gene library building and for subsequently
1073 sequencing these libraries at the MBSU facility.

1074 **Financial support**

1075 Funding and support were provided to D. Olefeldt and M. Bhatia by the Natural Science and
1076 Engineering Research Council of Canada, Discovery grant (RGPIN-2016-04688 to DO and
1077 RGPIN-2020-05975 to MB) and the Campus Alberta Innovates Program (CAIP).

1078

1079

1080

1081 **References**

1082 Adamczyk, M., Perez-Mon, C., Gunz, S., & Frey, B. (2020). Strong shifts in microbial
1083 community structure are associated with increased litter input rather than temperature in High

1084 Arctic soils. *Soil Biology and Biochemistry*, 151.
1085 <https://doi.org/10.1016/j.soilbio.2020.108054>
1086
1087 Allan, E., Manning, P., Alt, F., Binkenstein, J., Blaser, S., Blüthgen, N., ... Fischer, M.
1088 (2015). Land use intensification alters ecosystem multifunctionality via loss of
1089 biodiversity and changes to functional composition. *Ecology Letters*.
1090 <https://doi.org/10.1111/ele.12469>
1091
1092 [Baltzer JL, Veness T, Chasmer LE, et al \(2014\) Forests on thawing permafrost:](#)
1093 [fragmentation, edge effects, and net forest loss. *Global Change Biology* 20:824–834. doi:](#)
1094 [10.1111/gcb.12349](#)
1095
1096 [Bauer, I. E., Gignac, L. D., & Vitt, D. H. \(2003\). Development of a peatland complex in](#)
1097 [boreal western Canada: Lateral site expansion and local variability in vegetation succession](#)
1098 [and long-term peat accumulation. *Canadian Journal of Botany*, 81\(8\), 833–847.](#)
1099 <https://doi.org/10.1139/b03-076>
1100
1101 Beilman, D. W. (2001). Plant community and diversity change due to localized permafrost
1102 dynamics in bogs of western Canada. *Canadian Journal of Botany*, 79(8), 983–993.
1103 <https://doi.org/10.1139/cjb-79-8-983>
1104
1105 Bellisario, L. M., Bubier, J. L., Moore, T. R., & Chanton, J. P. (1999). Controls on CH₄
1106 emissions from a northern peatland. *Global Biogeochemical Cycles*, 13(1).
1107 <https://doi.org/10.1029/1998GB900021>
1108
1109 Berghuis, B.A., Yu, F.B., Schulz, F., Blainey, P.C., Woyke, T., Quake, S.R. (2019).
1110 Hydrogenotrophic methanogenesis in archaeal phylum Verstraetearchaeota reveals the shared
1111 ancestry of all methanogens. *PNAS* 116 (11): 5037-5044.
1112 <https://doi.org/10.1073/pnas.1815631116>
1113
1114 Blodau, C., Basiliko, N., ~~&~~ Moore, T. R. (2004). Carbon turnover in peatland
1115 mesocosms exposed to different water table levels. *Biogeochemistry*.
1116 https://doi.org/10.1023/B:BIOG.0000015788.30164.e_2
1117
1118 [Boon, E., Meehan, C. J., Whidden, C., Wong, D. H., Langille, M. G., & Beiko, R. G. \(2014\).](#)
1119 [Interactions in the microbiome: communities of organisms and communities of genes. *FEMS*](#)
1120 [microbiology reviews, 38\(1\), 90–118. <https://doi.org/10.1111/1574-6976.12035>](#)
1121
1122 [Bragazza, L., Bardgett, R. D., Mitchell, E. A. D., & Buttler, A. \(2015\). Linking soil microbial](#)
1123 [communities to vascular plant abundance along a climate gradient. *New Phytologist*, 205\(3\),](#)
1124 [1175–1182. <https://doi.org/10.1111/nph.13116>](#)
1125

1126 Bridgham, S. D., Cadillo-Quiroz, H., Keller, J. K., & Zhuang, Q. (2013). Methane
1127 emissions from wetlands: Biogeochemical, microbial, and modeling perspectives from local
1128 to global scales. *Global Change Biology*. <https://doi.org/10.1111/gcb.12131>
1129

1130 Brown, J., Ferrians Jr., O. J., Heginbottom, J. A., & Melnikov, E. S. (1997). Circum-
1131 Arctic map of permafrost and ground ice conditions. USGS Numbered Series, 1.
1132 <https://doi.org/10.1016/j.jallcom.2010.03.054>
1133

1134 Burd, K., Estop-Aragónés, C., Tank, S. E., & Olefeldt, D. (2020). Lability of dissolved
1135 organic carbon from boreal peatlands: interactions between permafrost thaw, wildfire,
1136 and season. *Canadian Journal of Soil Science*, 13(February), 1–13.
1137 <https://doi.org/10.1139/cjss-2019-0154>
1138

1139 Burger, M., Berger, S., Spangenberg, I., Blodau, C. (2016). Summer fluxes of methane and
1140 carbon dioxide from a pond and floating mat in a continental Canadian peatland.
1141 *Biogeosciences*. 13: 3777-3791. <https://doi.org/10.5194/bg-13-3777-2016>.
1142

1143 Cai, L., Alexeev, V.A., Arp, C.D., Jones, B.M., Liljedahl, A., Gadeke, A. (2016). Dynamical
1144 Downscaling data for studying climactic impacts on hydrology, permafrost and ecosystem sin
1145 Arctic Alaska. *Earth System Science Data Discussion*, doi:10.5194/tc-2016-87
1146

1147 Camill, P. (1999). Peat accumulation and succession following permafrost thaw in the Boreal
1148 peatlands of Manitoba, Canada. *Ecoscience*, 6(4), 592–602.
1149 <https://doi.org/10.1080/11956860.1999.11682561>
1150

1151 Carrigg, C., Rice, O., Kavanagh, S., Collins, G., O’Flaherty, V. (2007). DNA extraction
1152 method affects microbial community profiles from soils and sediment. *Applied Microbiology
1153 and Biotechnology* 77(4), 955-964.

1154 Carroll, P., & Crill, P. (1997). Carbon balance of a temperate poor fen. *Global
1155 Biogeochemical Cycles*. <https://doi.org/10.1029/97GB01365>
1156

1157 [Carson, M.A, Bräuer, S., Basiliko, N.,\(2019\). Enrichment of peat yields novel methanogens:
1158 approaches for obtaining uncultured organisms in the age of rapid sequencing, *FEMS
1159 Microbiology Ecology*, 95\(2\): <https://doi.org/10.1093/femsec/fiz001>
1160](https://doi.org/10.1093/femsec/fiz001)

1161 Chanton, J., Chaser, L., Glasser, P., & Siegel, D. (2005). Carbon and Hydrogen Isotopic
1162 Effects in Microbial, Methane from Terrestrial Environments. *Stable Isotopes and
1163 Biosphere - Atmosphere Interactions*, 85–105. [https://doi.org/10.1016/B978-012088447-
1164 6/50006-4](https://doi.org/10.1016/B978-012088447-6/50006-4)
1165

1166 Chanton, J. P., Glaser, P. H., Chasar, L. S., Burdige, D. J., Hines, M. E., Siegel, D. I., ...
1167 Cooper, W. T. (2008). Radiocarbon evidence for the importance of surface vegetation on
1168 fermentation and methanogenesis in contrasting types of boreal peatlands. *Global
1169 Biogeochemical Cycles*, 22(4), 1–11. <https://doi.org/10.1029/2008GB003274>

1170 Climate-Data.org. (2019). Retrieved January 21, 2019, from 2019 website:
1171 <https://en.climate-data.org/north-america/canada/alberta/meander-river-11380/>
1172

1173 [Chasar, L. S., Chanton, J. P., Glaser, P. H., Siegel, D. I., and Rivers, J. S. \(2000\),](#)
1174 [Radiocarbon and stable carbon isotopic evidence for transport and transformation of](#)
1175 [dissolved organic carbon, dissolved inorganic carbon, and CH₄ in a northern Minnesota](#)
1176 [peatland, *Global Biogeochem. Cycles*, 14\(4\), 1095– 1108, doi:10.1029/1999GB001221.](#)
1177

1178 [Chasmer, L. and Hopkinson, C. \(2017\), Threshold loss of discontinuous permafrost and](#)
1179 [landscape evolution. *Glob Change Biol*, 23: 2672-2686. <https://doi.org/10.1111/gcb.13537>](#)
1180

1181 [Cooper, M. D. A., Estop-Aragonés, C., Fisher, J. P., Thierry, A., Garnett, M. H., Charman, D.](#)
1182 [J., et al. \(2017\). Limited contribution of permafrost carbon to methane release from thawing](#)
1183 [peatlands. *Nature Climate Change*, 7\(7\), 507–511. <https://doi.org/10.1038/nclimate3328>](#)
1184

1185 Comte, J., Monier, A., Crevecoeur, S., Lovejoy, C., Vincent, W.F.(2015). Microbial
1186 biogeography of permafrost thaw ponds across the changing northern landscape. *Ecography*
1187 39, 609-618.
1188

1189 Connon, R.F., Quinton, W.L., Craig, J.R., Hayashi, M. (2014). Changing hydrologic
1190 connectivity due to permafrost thaw in the lower Liard River valley, NWT, Canada.
1191 *Hydrological Processes* 28(14): 4163-4178. <https://doi.org/10.1002/hyp.10206>
1192

1193 Conrad, R. (1999). Contribution of hydrogen to methane production and control of hydrogen
1194 concentrations in methanogenic soils and sediments. *FEMS Microbiology Ecology*.
1195 [https://doi.org/10.1016/S0168-6496\(98\)00086-5](https://doi.org/10.1016/S0168-6496(98)00086-5)
1196

1197 Corbett, J. E., Tfaily, M. M., Burdige, D. J., Cooper, W. T., Glaser, P. H., & Chanton, J.
1198 P. (2013). Partitioning pathways of CO₂ production in peatlands with stable carbon
1199 isotopes. *Biogeochemistry*, 114(1–3). <https://doi.org/10.1007/s10533-012-9813-1>
1200

1201 Criquet, S., Farnet, A. M., Tagger, S., & Le Petit, J. (2000). Annual variations of
1202 phenoloxidase activities in an evergreen oak litter: Influence of certain biotic and abiotic
1203 factors. *Soil Biology and Biochemistry*. [https://doi.org/10.1016/S0038-0717\(00\)00027-4](https://doi.org/10.1016/S0038-0717(00)00027-4)
1204

1205 Dunn, C., Jones, T.G, Girard, A., Freeman, C. (2014). Methodologies for Extracellular
1206 enzyme assays from wetland soils. *Wetlands* 34: 9-17 . [https://doi.org/10.1007/s13157-013-](https://doi.org/10.1007/s13157-013-0475-0)
1207 [0475-0.](https://doi.org/10.1007/s13157-013-0475-0)
1208

1209 Ebrahimi, A., & Or, D. (2017). Mechanistic modeling of microbial interactions at pore to
1210 profile scale resolve methane emission dynamics from permafrost soil. *Journal of*
1211 *Geophysical Research: Biogeosciences*, 122(5). <https://doi.org/10.1002/2016JG003674>
1212

1213 [Estop-Aragónés, C., Czimeczik, C. I., Heffernan, L., Gibson, C., Walker, J. C., Xu, X., &](#)
1214 [Olefeldt, D. \(2018\). Respiration of aged soil carbon during fall in permafrost peatlands](#)
1215 [enhanced by active layer deepening following wildfire but limited following thermokarst.](#)
1216 [Environmental Research Letters, 13\(8\). <https://doi.org/10.1088/1748-9326/aad5f0>](#)
1217

1218 Euskirchen, E. S., Edgar, C. W., Turetsky, M. R., Waldrop, M. P., & Harden, J. W.
1219 (2014). Differential response of carbon fluxes to climate in three peatland ecosystems that
1220 vary in the presence and stability of permafrost. *Journal of Geophysical Research G:*
1221 *Biogeosciences*. <https://doi.org/10.1002/2014JG002683>
1222

1223 Feng, J., Wang, C., Lei, J., Yang, Y., Yan, Q., Zhou, X...Zhou, J. (2020). Warming-induced
1224 permafrost thaw exacerbates tundra soil carbon decomposition mediated by microbial
1225 community. *Microbiome* 8(3), <https://doi.org/10.1186/s40168-019-0778-3>
1226

1227 Fisher, R. E., France, J. L., Lowry, D., Lanoisellé, M., Brownlow, R., Pyle, J. A., ... Nisbet,
1228 E. G. (2017). Measurement of the ¹³C isotopic signature of methane emissions from northern
1229 European wetlands. *Global Biogeochemical Cycles*, 31(3).
1230 <https://doi.org/10.1002/2016GB005504>
1231

1232 Fox, J., & Weisberg, S. (2011). *An R Companion to Applied Regression*, second ed.
1233 <https://doi.org/10.1016/j.stomax.2010.07.001>
1234

1235 Frey, B., Rime, T., Phillips, M., Stierli, B., Hajdas, I., Widmer, F., Hartmann, M. (2016).
1236 Microbial diversity in European alpine permafrost nad active layers. *FEMS microbiology*
1237 *Ecology*. 92: doi.org/10.1093/femsec/fiw018
1238

1239 Fritze, H., Penttilä, T., Mäkiranta, P., Laiho, R., Tuomivirta, T., Forsman, J., ... Peltoniemi,
1240 K. (2021). Exploring the mechanisms by which reindeer droppings induce fen peat methane
1241 production. *Soil Biology and Biochemistry*, 160.
1242 <https://doi.org/10.1016/j.soilbio.2021.108318>
1243

1244 [Galand, P. E., Fritze, H., Conrad, R., & Yrjälä, K. \(2005\). Pathways for methanogenesis and](#)
1245 [diversity of methanogenic archaea in three boreal peatland ecosystems. *Applied and*](#)
1246 [environmental microbiology, 71\(4\), 2195–2198. \[https://doi.org/10.1128/AEM.71.4.2195-\]\(https://doi.org/10.1128/AEM.71.4.2195-2198.2005\)](#)
1247 [2198.2005](#)

1248

1249 Gibson, C. M., Chasmer, L. E., Thompson, D. K., Quinton, W. L., Flannigan, M. D., &
1250 Olefeldt, D. (2018). Wildfire as a major driver of recent permafrost thaw in boreal
1251 peatlands. *Nature Communications*, 9(1). <https://doi.org/10.1038/s41467-018-05457-1>
1252

1253 Grant, R. F. (2015). Ecosystem CO₂ and CH₄ exchange in a mixed tundra and a fen within a
1254 hydrologically diverse Arctic landscape: 2. Modeled impacts of climate change. *Journal of*
1255 *Geophysical Research: Biogeosciences*, 120(7). <https://doi.org/10.1002/2014JG002889>
1256

1257 [Hädrieh, Anke., Heuer, Verena B., Herrmann, Martina., Hinrichs, Kai-Uwe., Küsel, Kirsten.,](#)
1258 [Origin and fate of acetate in an acidic fen, FEMS Microbiology Ecology, Volume 81, Issue 2,](#)
1259 [August 2012, Pages 339–354, <https://doi.org/10.1111/j.1574-6941.2012.01352.x>](#)
1260

1261 [Hamberger A, Horn MA, Dumont MG, Murrell JC & Drake HL \(2008\) Anaerobic consumers](#)
1262 [of monosaccharides in a moderately acidic fen. Appl Environ Microbiol 74: 3112–3120.](#)
1263

1264 Hansen, A. M., Kraus, T. E. C., Pellerin, B. A., Fleck, J. A., Downing, B. D., & Bergamaschi,
1265 B. A. (2016). Optical properties of dissolved organic matter (DOM): Effects of biological and
1266 photolytic degradation. *Limnology and Oceanography*. <https://doi.org/10.1002/lno.10270>
1267

1268 Heffernan, L., Estop-Aragónés, C., Knorr, K.-H., Talbot, J., & Olefeldt, D. (2020).
1269 Long-term impacts of permafrost thaw on carbon storage in peatlands: deep losses offset by
1270 surficial accumulation. *Journal of Geophysical Research: Biogeosciences*, 2011(2865),
1271 e2019JG005501. <https://doi.org/10.1029/2019JG005501>
1272

1273 Heffernan, L., Jasey, V.E.J., Frederickson, M., Mackenzie, M.D., Olefeldt, D. (2021).
1274 Constraints on potential enzyme activities in thermokarst bogs: Implications for the carbon
1275 balance of peatlands following thaw. *Global Change Biology*, 27(19): 4711-4726.
1276 <https://doi.org/10.1111/gcb.15758>
1277

1278 Heginbottom, J. A., Dubreuil, M. H., & Harker, P. T. (1995). Canada, Permafrost. National
1279 Atlas of Canada.
1280

1281 Helbig, M., Pappas, C., & Sonnentag, O. (2016). Permafrost thaw and wildfire: Equally
1282 important drivers of boreal tree cover changes in the Taiga Plains, Canada. *Geophysical*
1283 *Research Letters*. <https://doi.org/10.1002/2015GL067193>
1284

1285 Helms, J.R., Stubbins, A., Ritchie, J.D., Minor, E.C., Kieber, D.J., Mopper, K. (2008).
1286 Absorption spectral slopes and slope ratios as indicators of molecular weight, source, and
1287 photobleaching of chromophoric dissolved organic matter. *Limnology and Oceanography*,
1288 53(3): 955-969. <https://doi.org/10.4319/lo.2008.53.3.0955>
1289

1290 Hodgkins, S. B., Tfaily, M. M., McCalley, C. K., Logan, T. A., Crill, P. M., Saleska, S. R., ...
1291 Chanton, J. P. (2014). Changes in peat chemistry associated with permafrost thaw
1292 increase greenhouse gas production. *Proceedings of the National Academy of Sciences*,
1293 111(16), 5819–5824. <https://doi.org/10.1073/pnas.1314641111>
1294

1295 Hoffman, G.E., Schadt, E.E. (2016). variancePartition: interpreting drivers of variance in
1296 complex gene expression studies. *BMC bioinformatics* 17(483).
1297 <https://doi.org/10.1186/s12859-016-1323-z>.
1298

1299 Holm, S., Walz, J., Horn, F., Yang, S., Grigoriev, M. N., Wagner, D., ... Liebner, S. (2020).
1300 Methanogenic response to long-term permafrost thaw is determined by

1301 paleoenvironment. *FEMS Microbiology Ecology*, 96(3).
1302 <https://doi.org/10.1093/femsec/fiaa021>
1303
1304 Hopple, A. M., Wilson, R. M., Kolton, M., Zalman, C. A., Chanton, J. P., Kostka, J., ...
1305 Bridgham, S. D. (2020). Massive peatland carbon banks vulnerable to rising
1306 temperatures. *Nature Communications*, 11(1). [https://doi.org/10.1038/s41467-020-](https://doi.org/10.1038/s41467-020-16311-8)
1307 [16311-8](https://doi.org/10.1038/s41467-020-16311-8)
1308
1309 Hornibrook, E. R. C., Longstaffe, F. J., & Fyfe, W. S. (1997). Spatial distribution of
1310 microbial methane production pathways in temperate zone wetland soils: Stable carbon
1311 and hydrogen isotope evidence. *Geochimica et Cosmochimica Acta*, 61(4), 745–753.
1312 [https://doi.org/https://doi.org/10.1016/S0016-7037\(96\)00368-7](https://doi.org/10.1016/S0016-7037(96)00368-7)
1313
1314 Hornibrook, E. R. C., Longstaffe, F. J., & Fyfe, W. S. (2000). Evolution of stable carbon
1315 isotope compositions for methane and carbon dioxide in freshwater wetlands and other
1316 anaerobic environments. *Geochimica et Cosmochimica Acta*, 64(6).
1317 [https://doi.org/10.1016/S0016-7037\(99\)00321-X](https://doi.org/10.1016/S0016-7037(99)00321-X)
1318
1319 Hough, M., McClure, A., Bolduc, B., Dorrepaal, E., Saleska, S., Klepac-Ceraj, V., Rich, V.
1320 (2020). Biotic and environmental drivers of plant microbiomes across a permafrost thaw
1321 gradient. *Frontiers in Microbiology*: <https://doi.org/10.3389/fmicb.2020.00796>
1322
1323 Huang, Y., Ciais, P., Luo, Y., Zhu, D., Wang, Y., Qiu, C., ... Qu, L. (2021). Tradeoff of CO₂
1324 and CH₄ emissions from global peatlands under water-table drawdown. *Nature Climate*
1325 *Change*, 11(7). <https://doi.org/10.1038/s41558-021-01059-w>
1326
1327 [Hugelius, G., Strauss, J., Zubrzycki, S., Harden, J. W., Schuur, E. A. G., Ping, C. L., ...](https://doi.org/10.5194/bg-11-6573-2014)
1328 [Kuhry, P. \(2014\). Estimated stocks of circumpolar permafrost carbon with quantified](https://doi.org/10.5194/bg-11-6573-2014)
1329 [uncertainty ranges and identified data gaps. *Biogeosciences*, 11\(23\), 6573–6593.](https://doi.org/10.5194/bg-11-6573-2014)
1330 <https://doi.org/10.5194/bg-11-6573-2014>
1331
1332 [Hugelius, G., Loisel, J., Chadburn, S., Jackson, R. B., Jones, M., MacDonald, G.,](https://doi.org/10.1073/pnas.1916387117)
1333 [Marushchak, M., Olefeldt, D., Packalen, M., Siewert, M. B., Treat, C., Turetsky, M., Voigt,](https://doi.org/10.1073/pnas.1916387117)
1334 [C., & Yu, Z. \(2020\). Large stocks of peatland carbon and nitrogen are vulnerable to](https://doi.org/10.1073/pnas.1916387117)
1335 [permafrost thaw. *Proceedings of the National Academy of Sciences of the United States of*](https://doi.org/10.1073/pnas.1916387117)
1336 [*America*, 117\(34\), 20438–20446. https://doi.org/10.1073/pnas.1916387117](https://doi.org/10.1073/pnas.1916387117)
1337
1338 ~~[Hugelius, G., Strauss, J., Zubrzycki, S., Harden, J. W., Schuur, E. A. G., Ping, C. L., ...](https://doi.org/10.5194/bg-11-6573-2014)~~
1339 ~~[Kuhry, P. \(2014\). Estimated stocks of circumpolar permafrost carbon with quantified](https://doi.org/10.5194/bg-11-6573-2014)~~
1340 ~~[uncertainty ranges and identified data gaps. *Biogeosciences*, 11\(23\), 6573–6593.](https://doi.org/10.5194/bg-11-6573-2014)~~
1341 ~~<https://doi.org/10.5194/bg-11-6573-2014>~~
1342
1343 Jassey, V. E. J., Chiapusio, G., Gilbert, D., Toussaint, M. L., & Binet, P. (2012).

1344 Phenoloxidase and peroxidase activities in Sphagnum-dominated peatland in a warming
1345 climate. *Soil Biology and Biochemistry*, 46, 49–52.
1346 <https://doi.org/10.1016/j.soilbio.2011.11.011>
1347

1348 Johnston, C. E., Ewing, S. A., Harden, J. W., Varner, R. K., Wickland, K. P., Koch, J. C., ...
1349 Jorgenson, M. T. (2014). Effect of permafrost thaw on CO₂ and CH₄ exchange in a
1350 western Alaska peatland chronosequence. *ENVIRONMENTAL RESEARCH LETTERS*,
1351 9(8). <https://doi.org/10.1088/1748-9326/9/8/085004>
1352

1353 Jones, M. C., Harden, J., O'Donnell, J., Manies, K., Jorgenson, T., Treat, C., & Ewing,
1354 S. (2018). Rapid carbon loss and slow recovery following permafrost thaw in boreal
1355 peatlands. *Global Change Biology*, 23(3), 1109–1127. <https://doi.org/10.1111/gcb.13403>
1356

1357 Juottonen, H., Kieman, M., Fritze, H., Hamberg, L., Laine, A. M., Merilä, P., ... Tuittila, E.
1358 S. (2021). Integrating Decomposers, Methane-Cycling Microbes and Ecosystem Carbon
1359 Fluxes Along a Peatland Successional Gradient in a Land Uplift Region. *Ecosystems*.
1360 <https://doi.org/10.1007/s10021-021-00713-w>
1361

1362 Kammann, C., Grünhage, L., & Jäger, H. J. (2001). A new sampling technique to
1363 monitor concentrations of CH₄, N₂O and CO₂ in air at well-defined depths in soils with
1364 varied water potential. *European Journal of Soil Science*, 52(2).
1365 <https://doi.org/10.1046/j.1365-2389.2001.00380.x>
1366

1367 Kassambara, A., & Mundt, F. (2017). Package “factoextra.” R Topics Documented.
1368

1369 Kassambara, A. (2018). ggpubr: “ggplot2” Based Publication Ready Plots. R package version
1370 0.2. <https://CRAN.R-project.org/package=ggpubr>. [https://CRAN.R-](https://CRAN.R-project.org/package=ggpubr)
1371 [Project.Org/Package=ggpubr. https://doi.org/R package version 0.1.8](https://doi.org/R%20package%20version%200.1.8)
1372

1373 Keeling, C. D. (1958). The concentration and isotopic abundances of atmospheric carbon
1374 dioxide in rural areas. *Geochimica et Cosmochimica Acta*, 13(4).
1375 [https://doi.org/10.1016/0016-7037\(58\)90033-4](https://doi.org/10.1016/0016-7037(58)90033-4)
1376

1377 [Kendall M.M., Boone D.R. \(2006\). Cultivation of methanogens from shallow marine](#)
1378 [sediments at Hydrate Ridge, Oregon. *Archaea*.2\(1\): 31-8. doi: 10.1155/2006/710190. PMID:](#)
1379 [16877319; PMCID: PMC2685590.](#)
1380

1381 Keuper, F., van Bodegom, P.M., Dorrepaal, E., Weedon, J.T., van Hal, J., van Logtestijn, R.
1382 S.P., Aerts, R. (2012). A frozen feast: thawing permafrost increases plant-available
1383 nitrogen in subarctic peatlands. *Global Change Biology*, 18(6) :1998-2007.
1384 <https://doi.org/10.1111/j.1365-2486.2012.02663.x>
1385

1386 Keuper, F., Dorrepaal, E., van Bodegom, P.M., van Logtestijn, R., Venhuizen, G., van Hal, J.,
1387 Aerts, R. (2017). Experimentally increased nutrient availability at the permafrost thaw front

1388 selectively enhances biomass production of deep-rooting subarctic peatland species. *Global*
1389 *Change Biology* 23(10) : 4257-4266. doi: 10.1111/gcb.13804
1390

1391 Kirkwood, J. A. H., Roy-Léveillé, P., Mykytczuk, N., Packalen, M., McLaughlin, J.,
1392 Laframboise, A., & Basiliko, N. (2021). Soil Microbial Community Response to Permafrost
1393 Degradation in Palsa Fields of the Hudson Bay Lowlands: Implications for Greenhouse Gas
1394 Production in a Warming Climate. *Global Biogeochemical Cycles*, 35(6).
1395 <https://doi.org/10.1029/2021GB006954>
1396

1397 Knoblauch, C., Beer, C., Liebner, S., Grigoriev, M.N., Pfeiffer, E.M. (2018). Methane
1398 production as key to the greenhouse gas budget of thawing permafrost. *Nature Climate*
1399 *Change*, 8, 309-312. <https://doi.org/10.1038/s41558-018-0095-z>
1400

1401 Knorr, K. H., Lischeid, G., & Blodau, C. (2009). Dynamics of redox processes in a
1402 minerotrophic fen exposed to a water table manipulation. *Geoderma*, 153(3–4).
1403 <https://doi.org/10.1016/j.geoderma.2009.08.023>
1404

1405 [Kotiaho, M., Fritze, H., Merilä, P. et al. Actinobacteria community structure in the peat](#)
1406 [profile of boreal bogs follows a variation in the microtopographical gradient similar to](#)
1407 [vegetation. *Plant Soil* 369, 103–114 \(2013\). <https://doi.org/10.1007/s11104-012-1546-3>](#)
1408

1409 Kotsyurbenko, O. R., Friedrich, M. W., Simankova, M. V., Nozhevnikova, A. N., Golyshin,
1410 P. N., Timmis, K. N., & Conrad, R. (2007). Shift from acetoclastic to H₂-dependent
1411 methanogenesis in a West Siberian peat bog at low pH values and isolation of an
1412 acidophilic *Methanobacterium* strain. *Applied and Environmental Microbiology*, 73(7),
1413 2344–2348. <https://doi.org/10.1128/AEM.02413-06>
1414

1415 [Kotsyurbenko, O.R., \(2005\). Trophic interactions in the methanogenic microbial community](#)
1416 [of low-temperature terrestrial ecosystems, *FEMS Microbiology Ecology*. , Volume 53\(, Issue](#)
1417 [1\); June 2005, Pages 3–13, <https://doi.org/10.1016/j.femsec.2004.12.009>](#)
1418

1419 Kuhn, M., Varner, R., Bastviken, D., Crill, P., MacIntyre, S., Turetsky, M., ... Olefeldt, D.
1420 (2021). BAWLD-CH₄: A Comprehensive Dataset of Methane
1421 Fluxes from Boreal and Arctic Ecosystems. *Earth System Science Data Discussions*.
1422 <https://doi.org/10.5194/essd-2021-141>
1423

1424 [Kuhry, Peter \(2008\). Vegetation cover and radiocarbon dates of palsa and peat plateaus in the](#)
1425 [Hudson Bay Lowlands. *PANGAEA*, <https://doi.org/10.1594/PANGAEA.812224>,](#)
1426 [Supplement to: Kuhry, P \(2008\): Palsa and peat plateau development in the Hudson Bay](#)
1427 [Lowlands, Canada: timing, pathways and causes. *Boreas*, 37\(2\), 316-327,](#)
1428 [<https://doi.org/10.1111/j.1502-3885.2007.00022.x>](#)
1429

1430 Kujala, K., Seppälä, M., & Holappa, T. (2008). Physical properties of peat and palsa
1431 formation. *Cold Regions Science and Technology*, 52(3).
1432 <https://doi.org/10.1016/j.coldregions.2007.08.002>
1433

1434 Lee, H., Schuur, E. A. G., Inglett, K. S., Lavoie, M., & Chanton, J. P. (2012). The rate of
1435 permafrost carbon release under aerobic and anaerobic conditions and its potential
1436 effects on climate. *Global Change Biology*, 18(2). [https://doi.org/10.1111/j.1365-](https://doi.org/10.1111/j.1365-2486.2011.02519.x)
1437 [2486.2011.02519.x](https://doi.org/10.1111/j.1365-2486.2011.02519.x)
1438

1439 Leroy, F., Gogo, S., Guimbaud, C., Bernard-Jannin, L., Hu, Z., & Laggoun-Déferge, F.
1440 (2017). Vegetation composition controls temperature sensitivity of CO₂ and CH₄ emissions
1441 and DOC concentration in peatlands. *Soil Biology and Biochemistry*, 107.
1442 <https://doi.org/10.1016/j.soilbio.2017.01.005>
1443

1444 Liebner, S., Ganzert, L., Kiss, A., Yang, S., Wagner, D., & Svenning, M. M. (2015).
1445 Shifts in methanogenic community composition and methane fluxes along the degradation of
1446 discontinuous permafrost. *Frontiers in Microbiology*, 6(MAY).
1447 <https://doi.org/10.3389/fmicb.2015.00356>
1448

1449 [Lin, Y., Liu, D., Yuan, J., Ye, G, Ding, W. \(2017\). Methanogenic community was stable in](https://doi.org/10.3389/fmicb.2017.00932)
1450 [two contrasting freshwater marshes exposed to elevated atmospheric CO₂. *Front Microbiol.*](https://doi.org/10.3389/fmicb.2017.00932)
1451 <https://doi.org/10.3389/fmicb.2017.00932>
1452

1453 Luláková, P., Perez-Mon, C., Šantrůčková, H., Ruethi, J., & Frey, B. (2019). High-
1454 alpine permafrost and active-layer soil microbiomes differ in their response to elevated
1455 temperatures. *Frontiers in Microbiology*, 10(APR). <https://doi.org/10.3389/fmicb.2019.00668>
1456

1457 Masella, A. P., Bartram, A. K., Truszkowski, J. M., Brown, D. G., & Neufeld, J. D.
1458 (2012). PANDAseq : PAired-eND Assembler for Illumina sequences. (Figure 1), 1–7.
1459

1460 McCalley, C. K., Woodcroft, B. J., Hodgkins, S. B., Wehr, R. A., Kim, E. H., Mondav, R., ...
1461 Saleska, S. R. (2014). Methane dynamics regulated by microbial community response to
1462 permafrost thaw. *Nature*, 514(7253), 478–481. <https://doi.org/10.1038/nature13798>
1463

1464 McDonald, D., Price, M.N., Goodrich, J., Nawrocki, E.P., DeSantis, T.Z., Probst, A.,
1465 Andersen, G.L., Knight, R., Hugenholtz, P. (2012). An improved Greengenes taxonomy with
1466 explicit ranks for ecological and evolutionary analyses of bacteria and archaea. *ISME*
1467 *Journal* 6: 610-618. <https://doi.org/10.1038/ismej.2011.139>
1468

1469 [McNicol, G., Knox, S.H., Guilderson, T.P., Baldocchi, D.D., Silver, W.L. \(2019\). Where old](https://doi.org/10.1111/gcb.14541)
1470 [meets new: An ecosystem study of methanogenesis in a reflooded agricultural peatland.](https://doi.org/10.1111/gcb.14541)
1471 [Global Change Biology 26\(2\):772-785.](https://doi.org/10.1111/gcb.14541)
1472

1473 Monteux, S., Weedon, J. T., Blume-Werry, G., Gavazov, K., Jassey, V. E. J., Johansson, M.,

1474 ... Dorrepaal, E. (2018). Long-term in situ permafrost thaw effects on bacterial
1475 communities and potential aerobic respiration. *ISME Journal*. [https://doi.org/10.1038/s41396-](https://doi.org/10.1038/s41396-018-0176-z)
1476 [018-0176-z](https://doi.org/10.1038/s41396-018-0176-z)
1477
1478 Mudryk, L., Brown, R., Derksen, C., Luo, J., Decharme, B., & Helfrich, S. (2018).
1479 Surface Air Temperature [in Arctic Report Card 2018]. Retrieved from
1480 <https://www.arctic.noaa.gov/Report-Card>
1481
1482
1483 Nielsen, C.S., Hasselquist, N.J., Nilsson, M.B., Öquist M., Järveoja J., Peichl M. (2019) .A
1484 Novel Approach for High-Frequency in-situ Quantification of Methane Oxidation in
1485 Peatlands. *Soil Systems* 3: 4
1486
1487 Oksanen, J., Blanchet, F. G., Kindt, R., Oksanen, M. J., & Suggests, M. (2013). Package
1488 ‘vegan.’ Community Ecology Package Version.
1489
1490 Olefeldt, D., Goswami, S., Grosse, G., Hayes, D., Hugelius, G., Kuhry, P., ... Turetsky, M.
1491 R. (2016). Circumpolar distribution and carbon storage of thermokarst landscapes.
1492 *Nature Communications*, 7, 13043. <https://doi.org/10.1038/ncomms13043>
1493
1494 Olefeldt, D., Euskirchen, E. S., Harden, J., Kane, E., McGuire, A. D., Waldrop, M. P., &
1495 Turetsky, M. R. (2017). A decade of boreal rich fen greenhouse gas fluxes in response to
1496 natural and experimental water table variability. *Global Change Biology*, 23(6), 2428–2440.
1497 <https://doi.org/10.1111/gcb.13612>
1498
1499 [Olefeldt, D., Heffernan, L., Jones, M. C., Sannel, A. B. K., Treat, C. C., & Turetsky, M. R.](#)
1500 [\(2021\). Permafrost thaw in northern peatlands: rapid changes in ecosystem and landscape](#)
1501 [functions. *Ecosystem Collapse and Climate Change*, 27-67.](#)
1502
1503 Parada, A. E., Needham, D. M., & Fuhrman, J. A. (2016). Every base ~~matters~~:
1504 assessing
1505 small subunit rRNA primers for marine microbiomes with mock ~~communities~~:
1506 communities.
1507 series and global field samples. *ISME Journal*, 18, 1403–1414. [https://doi.org/10.1111/1462-](https://doi.org/10.1111/1462-2920.13023)
1508 [2920.13023](https://doi.org/10.1111/1462-2920.13023)
1509
1510 Pelletier, N., Talbot, J., Olefeldt, D., Turetsky, M., Blodau, C., Sonnentag, O., & Quinton, W.
1511 L. (2017). Influence of Holocene permafrost aggradation and thaw on the paleoecology and
1512 carbon storage of a peatland complex in northwestern Canada. *Holocene*, 27(9), 1391–1405.
1513 <https://doi.org/10.1177/0959683617693899>
1514
1515 Perryman, C. R., McCalley, C. K., Malhotra, A., Fahnestock, M. F., Kashi, N. N., Bryce, J.
1516 G., ... Varner, R. K. (2020). Thaw Transitions and Redox Conditions Drive Methane
1517 Oxidation in a Permafrost Peatland. *Journal of Geophysical Research: Biogeosciences*,

1518 125(3). <https://doi.org/10.1029/2019JG005526>
1519
1520 Pinheiro J, Bates D, DebRoy S, S. D. and R. C. T. (2017). nlme: Linear and Nonlinear Mixed
1521 Effects Models. R package version 3.1-131, <https://CRAN.R-project.org/package=nlme>.
1522 R Package Version 3.1-131, <https://CRAN.R-Project.Org/Package=nlme>.
1523 <https://doi.org/10.1016/j.tibs.2011.05.003>
1524
1525 [Popp, T. J., Chanton, J. P., Whiting, G. J., and Grant, N. \(1999\), Methane stable isotope](#)
1526 [distribution at a Carex dominated fen in north central Alberta, *Global Biogeochem. Cycles*,](#)
1527 [13\(4\), 1063– 1077, doi:10.1029/1999GB900060.](#)
1528
1529 Preuss I, Knoblauch C, Gebert J & Pfeiffer EM (2013) Improved quantification of microbial
1530 CH₄ oxidation efficiency in arctic wetland soils using carbon isotope fractionation.
1531 *Biogeosciences* 10: 2539-2552
1532
1533 Quince, C., Lanzen, A., Davenport, R. J., & Turnbaugh, P. J. (2011). Removing Noise
1534 From Pyrosequenced Amplicons.
1535
1536 R Core Team. (2015). R: A language and environment for statistical computing. Vienna,
1537 Austria; 2014. URL [Http://Www. R-Project. Org](http://www.R-Project.Org). Vienna, Austria: R Foundation for
1538 Statistical Computing. <https://doi.org/10.1007/978-3-540-74686-7>
1539
1540 Robroek, B. J. M., Jassey, V. E. J., Kox, M. A. R., Berendsen, R. L., Mills, R. T. E., Cécillon,
1541 L., ... Bodelier, P. L. E. (2015). Peatland vascular plant functional types affect methane
1542 dynamics by altering microbial community structure. *Journal of Ecology*, 103(4).
1543 <https://doi.org/10.1111/1365-2745.12413>
1544
1545 Robroek, B. J. M., Martí, M., Svensson, B. H., Dumont, M. G., Veraart, A. J., & Jassey, V. E.
1546 J. (2021). Rewiring of peatland plant–microbe networks outpaces species turnover. *Oikos*,
1547 130(3). <https://doi.org/10.1111/oik.07635>
1548
1549 [Schädel, C., Bader, MF., Schuur, E. et al. Potential carbon emissions dominated by carbon](#)
1550 [dioxide from thawed permafrost soils. *Nature Clim Change* 6, 950–953 \(2016\).](#)
1551 <https://doi.org/10.1038/nclimate3054>
1552
1553 Schaefer, K., Zhang, T., Bruhwiler, L., & Barrett, A. P. (2011). Amount and timing of
1554 permafrost carbon release in response to climate warming. *Tellus, Series B: Chemical*
1555 *and Physical Meteorology*, 63(2). <https://doi.org/10.1111/j.1600-0889.2011.00527.x>
1556
1557 Schuur, E. A. G., McGuire, A. D., Schädel, C., Grosse, G., Harden, J. W., Hayes, D. J., ...
1558 Vonk, J. E. (2015). Climate change and the permafrost carbon feedback. *Nature*,
1559 520(7546), 171–179. <https://doi.org/10.1038/nature14338>
1560
1561 Simon, E., Canarini, A., Martin, V., Séneca, J., Böckle, T., Reinthaler, D., ... Richter, A.

1562 (2020). Microbial growth and carbon use efficiency show seasonal responses in a
1563 multifactorial climate change experiment. *Communications Biology*, 3(1).
1564 <https://doi.org/10.1038/s42003-020-01317-1>
1565

1566 Strack, M., Waddington, J. M., & Tuittila, E. S. (2004). Effect of water table drawdown on
1567 northern peatland methane dynamics: Implications for climate change. *Global*
1568 *Biogeochemical Cycles*. <https://doi.org/10.1029/2003GB002209>
1569

1570 Stams A.J.M., Teusink B., Sousa D.Z. (2019) Ecophysiology of Acetoclastic Methanogens.
1571 In: Stams A., Sousa D. (eds) *Biogenesis of Hydrocarbons. Handbook of Hydrocarbon and*
1572 *Lipid Microbiology*. Springer, Cham. https://doi.org/10.1007/978-3-319-78108-2_21
1573

1574 [Ström, L., Ekberg, A., Mastepanov, M. and Røjle Christensen, T. \(2003\), The effect of](#)
1575 [vascular plants on carbon turnover and methane emissions from a tundra wetland. *Global*](#)
1576 [Change Biology, 9: 1185-1192. <https://doi.org/10.1046/j.1365-2486.2003.00655.x>](#)
1577

1578 [Ström et al., \(2012\). Presence of *Eriophorum scheuchzeri* enhances substrate availability and](#)
1579 [methane emission in an Arctic wetland *Soil Biology and Biochemistry*, Volume 45, 2012,](#)
1580 [Pages 61-70, ISSN 0038-0717, <https://doi.org/10.1016/j.soilbio.2011.09.005>.](#)
1581

1582 Strom, L., Falk, J.M., Skov, K., Jackowicz-Korczynski, M., Mastepanov, M., Christensen, T.,
1583 Lund, M., Schmidt, N.M. (2015). Controls of spatial and temporal variability in CH₄ flux in a
1584 high arctic fen over three years. *Biogeochemistry* 125(1): 21-35.
1585

1586 [Treat, C. C., & Jones, M. C. \(2018\). Near-surface permafrost aggradation in Northern](#)
1587 [Hemisphere peatlands shows regional and global trends during the past 6000 years.](#)
1588 [Holocene. <https://doi.org/10.1177/0959683617752858>](#)
1589

1590 Turetsky, M. R., Wieder, R. K., Vitt, D. H., Evans, R. J., & Scott, K. D. (2007). The
1591 disappearance of relict permafrost in boreal north America: Effects on peatland carbon
1592 storage and fluxes. *Global Change Biology*, 13(9), 1922–1934.
1593 <https://doi.org/10.1111/j.1365-2486.2007.01381.x>
1594

1595 Turetsky, Merritt R., Abbott, B. W., Jones, M. C., Anthony, K. W., Olefeldt, D., Schuur, E.
1596 A. G., ... McGuire, A. D. (2020). Carbon release through abrupt permafrost thaw.
1597 *Nature Geoscience*. <https://doi.org/10.1038/s41561-019-0526-0>
1598

1599 Tuittila, E. S., Komulainen, V. M., Vasander, H., Nykanen, H., Martikainen, P. J., & Laine, J.
1600 (2000). Methane dynamics of a restored cut-away peatland. *Global Change Biology*, 6(5),
1601 569–581. <https://doi.org/10.1046/j.1365-2486.2000.00341.x>
1602

1603 [Vanwongerghem, I., Evans, P., Parks, D. et al. \(2016\). Methylotrophic methanogenesis](#)
1604 [discovered in the archaeal phylum Verstraetearchaeota. *Nat Microbiol* 1:](#)
1605 <https://doi.org/10.1038/nmicrobiol.2016.170>

1606
1607 [Vishnivetskaya, T.A., Buongiorno, J., Bird, J., Krivushin, K., Spirina, E.V., Oshurkova, V.,](#)
1608 [Shcherbakova, V.A., Wilson, G., Lloyd, K.G., Rivkina, E.M. \(2018\).Methanogens in the](#)
1609 [Antarctic Dry Valley permafrost, *FEMS Microbiology Ecology*, 94\(8\)](#)
1610 [fiy109, <https://doi.org/10.1093/femsec/fiy109>](#)
1611
1612 Vitt, D. H., Halsey, L. A., Bauer, I. E., & Campbell, C. (2000). Spatial and temporal trends in
1613 carbon storage of peatlands of continental western Canada through the Holocene.
1614 *Canadian Journal of Earth Sciences*, 37(5), 683–693. <https://doi.org/10.1139/e99-097>
1615
1616 Vitt, D. H., Halsey, L. A., & Zoltai, S. C. (1994). The Bog Landforms of Continental Western
1617 Canada in Relation to Climate and Permafrost Patterns. *Arctic and Alpine Research*,
1618 26(1), 1. <https://doi.org/10.2307/1551870>
1619
1620 Weishaar, J.L., Aiken, G.R., Bergamaschi, B.A., Fram, M.S., Fujii, R., Mopper, K. (2003).
1621 Evaluation of specific ultraviolet absorbance as an indicator of the chemical composition and
1622 reactivity of dissolved organic carbon. *Environmental Science and Technology* 37(20): 4702-
1623 4708. <https://doi.org/10.1021/es030360x>
1624
1625 Whiticar, M. J., Faber, E., & Schoell, M. (1986). Biogenic methane formation in marine and
1626 freshwater environments: CO₂ reduction vs. acetate fermentation-Isotope evidence.
1627 *Geochimica et Cosmochimica Acta*, 50(5). [https://doi.org/10.1016/0016-7037\(86\)90346-](https://doi.org/10.1016/0016-7037(86)90346-7)
1628 [7](https://doi.org/10.1016/0016-7037(86)90346-7)
1629
1630 Whiticar, Michael J. (1999). Carbon and hydrogen isotope systematics of bacterial formation
1631 and oxidation of methane. *Chemical Geology*, 161(1). [https://doi.org/10.1016/S0009-](https://doi.org/10.1016/S0009-2541(99)00092-3)
1632 [2541\(99\)00092-3](https://doi.org/10.1016/S0009-2541(99)00092-3)
1633
1634 Wickham, H. (2016). *ggplot2 -Positioning Elegant Graphics for Data Analysis*. In Springer.
1635
1636 Wickland, K. P., Striegl, R. G., Neff, J. C., & Sachs, T. (2006). Effects of permafrost melting
1637 on CO₂ and CH₄ exchange of a poorly drained black spruce lowland. *Journal of*
1638 *Geophysical Research: Biogeosciences*, 111(2), 1–13.
1639 <https://doi.org/10.1029/2005JG000099>
1640
1641 [Wüst, P.K., Horn, M.A. and Drake, H.L. \(2009\), Trophic links between fermenters and](#)
1642 [methanogens in a moderately acidic fen soil. *Environmental Microbiology*, 11: 1395-1409.](#)
1643 <https://doi.org/10.1111/j.1462-2920.2009.01867.x>
1644
1645 Ye, R., Jin, Q., Bohannon, B., Keller, J. K., McAllister, S. A., & Bridgham, S. D. (2012). PH
1646 controls over anaerobic carbon mineralization, the efficiency of methane production, and
1647 methanogenic pathways in peatlands across an ombrotrophic-minerotrophic gradient. *Soil*
1648 *Biology and Biochemistry*, 54, 36–47. <https://doi.org/10.1016/j.soilbio.2012.05.015>

1649

1650 [Zhang, C.J., Pan, J., Liu, Y. et al. \(2020\). Genomic and transcriptomic insights into](#)
1651 [methanogenesis potential of novel methanogens from mangrove sediments. Microbiome 8](#)
1652 [\(94 \): https://doi.org/10.1186/s40168-020-00876-z](#)

1653

1654 Zoltai, S. C. (1972). Palsas and Peat Plateaus in Central Manitoba and Saskatchewan.
1655 Canadian Journal of Forest Research, 2(3), 291–302. <https://doi.org/10.1139/x72-046>

1656

1657 Zoltai, S. C. (1993). Cyclic Development of Permafrost in the Peatlands of Northwestern
1658 Alberta, Canada. Arctic and Alpine Research, 25(3), 240.

1659 <https://doi.org/10.2307/1551820>